

## A Time-Resolved Spectroscopic Study of the Bichromophoric Phototrigger 3',5'-Dimethoxybenzoin Diethyl Phosphate: Interaction Between the Two Chromophores Determines the Reaction Pathway

Chensheng Ma,<sup>[a]</sup> Wai Ming Kwok,<sup>[b]</sup> Hui-Ying An,<sup>[a]</sup> Xiangguo Guan,<sup>[a]</sup>  
Michael Yunyi Fu,<sup>[a]</sup> Patrick H. Toy,<sup>[a]</sup> and David Lee Phillips\*<sup>[a]</sup>

**Abstract:** 3',5'-Dimethoxybenzoin (DMB) is a bichromophoric system that has widespread application as a highly efficient photoremovable protecting group (PRPG) for the release of diverse functional groups. The photodeprotection of DMB phototrigger is remarkably clean, and is accompanied by the formation of a biologically benign cyclization product, 3',5'-dimethoxybenzofuran (DMBF). The underlying mechanism of the DMB deprotection and cyclization has, however, until now remained unclear. Femtosecond transient absorption (fs-TA) spectroscopy and nanosecond time-resolved resonance Raman (ns-TR<sup>3</sup>) spectroscopy were employed to detect the transient species directly, and examine the dynamic transformations involved in the primary photoreactions for DMB diethyl phosphate (DMBDP) in acetonitrile (CH<sub>3</sub>CN). To assess the electronic character and the role played by the individual sub-chromophore, that is, the benzoyl, and the di-*meta*-methoxybenzylic moieties, for the DMBDP deprotection, comparative fs-TA measurements were also carried

out for the reference compounds diethyl phosphate acetophenone (DPAP), and 3',5'-dimethoxybenzylic diethyl phosphate (DMBnDP) in the same solvent. Comparison of the fs-TA spectra reveals that the photoexcited DMBDP exhibits distinctly different spectral character and dynamic evolution from those of the reference compounds. This fact, combined with the related steady-state spectral and density functional theoretical results, strongly suggests the presence in DMBDP of a significant interaction between the two sub-chromophores, and that this interaction plays a governing role in determining the nature of the photoexcitation and the reaction channel of the subsequent photophysical and photochemical transformations. The ns-TR<sup>3</sup> results and their correlation with the fs-TA spectra and dynamics provide evidence for a novel concerted deprotection–

cyclization mechanism for DMBDP in CH<sub>3</sub>CN. By monitoring the direct generation of the transient DMBF product, the cyclization time constant was determined unequivocally to be ≈ 1 ns. This indicates that there is little relevance for the long-lived intermediates (> 10 ns) in giving the DMBF product, and excludes the stepwise mechanism proposed in the literature as the major pathway for the DMB cyclization reaction. This work provides important new insights into the origin of the 3',5'-dimethoxy substitution effect for the DMB photodeprotection. It also helps to clarify the many different views presented in previous mechanistic studies of the DMB PRPGs. In addition to this, our fs-TA results on the reference compound DMBnDP in CH<sub>3</sub>CN provide the first direct observation (to the best of our knowledge) showing the predominance of a prompt (≈ 2 ps) heterolytic bond cleavage after photoexcitation of *meta*-methoxybenzylic compounds. This provides insight into the long-term controversies about the photoinitiated dissociation mode of related substituted benzylic compounds.

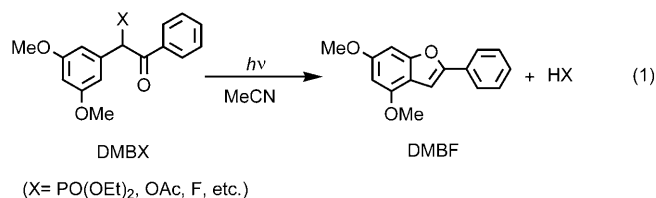
**Keywords:** chromophores · dimes-  
thoxybenzoin · photochemistry ·  
Raman spectroscopy · time-re-  
solved spectroscopy

[a] Dr. C. Ma, H.-Y. An, Dr. X. Guan, M. Y. Fu, Dr. P. H. Toy,  
Prof. D. L. Phillips  
Department of Chemistry, The University of Hong Kong  
Pokfulam Road, Hong Kong (P. R. China)  
Fax: (+852)2857-1586  
E-mail: phillips@hkucc.hku.hk

[b] Dr. W. M. Kwok  
Department of Applied Biology and Chemical Technology  
The Hong Kong Polytechnic University  
Hung Hom, Kowloon, Hong Kong (P. R. China)  
 Supporting information for this article is available on the WWW  
under <http://dx.doi.org/10.1002/chem.200902891>.

## Introduction

Because of the very efficient and biologically benign photoliberation of protected functional groups, 3',5'-dimethoxybenzoin (DMB) systems have been developed extensively as a photoremovable protecting group (PRPG) for many functional groups, such as inorganic phosphates,<sup>[1,2,3a]</sup> nucleotides,<sup>[2b,4]</sup> carboxylates,<sup>[5-7]</sup> amines,<sup>[3b,8]</sup> and alcohols.<sup>[3c]</sup> DMB has also found applications as a PRPG in drug delivery,<sup>[9]</sup> muscle relaxation studies,<sup>[10]</sup> lithographic synthesis,<sup>[3d]</sup> biochip fabrication,<sup>[3c,e]</sup> protein folding and unfolding,<sup>[11]</sup> and so forth. These practical applications of the DMB PRPG followed from pioneering studies by Sheehan and co-workers on benzoin esters and substituted analogues, which demonstrated the potential utilization of these compounds for the photorelease of carboxylic acid.<sup>[7]</sup> These and many other later studies on related benzoinyl derivatives have found a complex dependence of the photoproduct formation on a number of factors, including the character of the substituent(s) in the aromatic rings, the nature of the leaving group, and the properties of the solvent in which the reaction takes place, and so forth.<sup>[1-8,12,13]</sup> Among the broad range of photocoupling and addition reactions observed in many studies, the photoelimination along with cyclization of the benzoinyl group into the corresponding benzo[*b*]furan (BF) as an inert byproduct [Eq. (1)] constitutes one of the principal reactions for the photodeprotection of benzoin-based PRPG compounds. The efficiency of this reaction depends strongly on the substitution pattern on the benzylic ring, and when a twofold *meta*-methoxybenzylic substitution is employed, as in the DMB system, the photodeprotection and cyclization reactions become very clean and highly efficient. For instance, the photocyclization yield of DMB acetate is reported to be  $\approx 0.64$ ,<sup>[7a]</sup> which is more than twice the yield ( $\approx 0.26$ ) estimated for the corresponding unsubstituted benzoin acetate under similar deprotection conditions.<sup>[2a]</sup> This remarkable substituent effect suggests that DMB systems can be significantly superior compared to the nonsubstituted benzoin systems, and this accounts for the widespread application of DMB systems for use as PRPG compounds. However, the underlying reasons for this substantial substituent effect remain elusive, and there have been differing views on the reaction kinetics and mechanism(s) of the DMB photodeprotection.

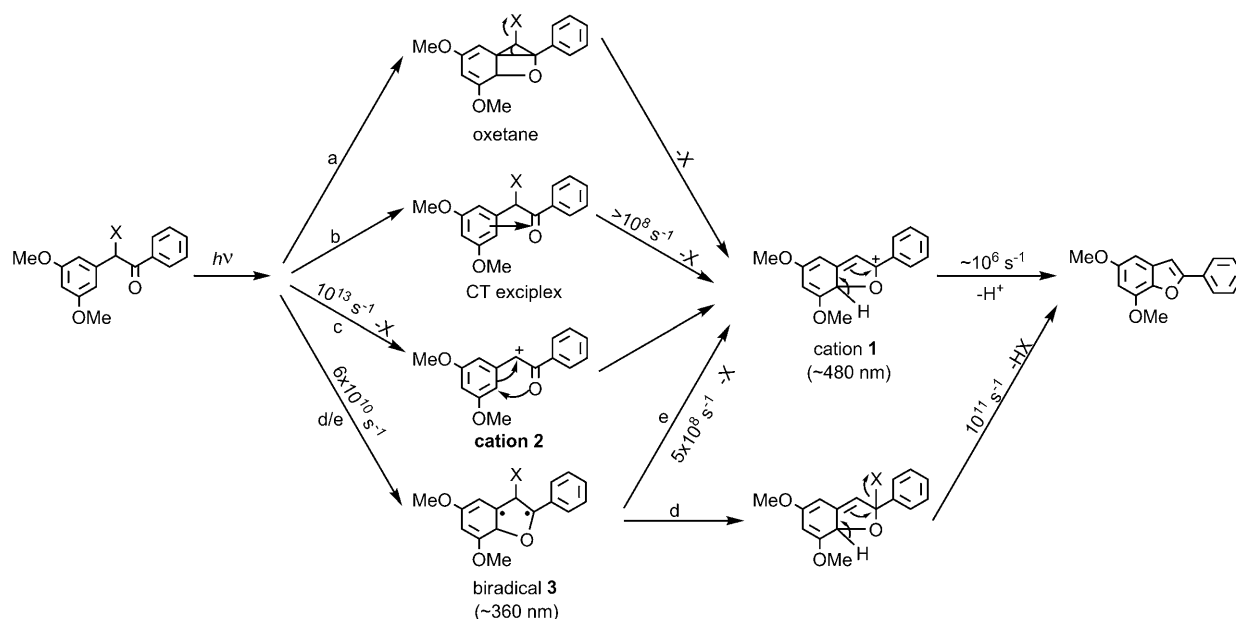


Previous mechanistic studies have revealed a clear description of the photodeprotection pathways for the parent benzoin system,<sup>[2a,13a]</sup> but the picture is not clear for the

DMB systems. Direct time-resolved transient absorption (TA)<sup>[2a,13a]</sup> and time-resolved resonance Raman (TR<sup>3</sup>)<sup>[13a]</sup> studies of a parent benzoin-based PRPG compound have provided solid pieces of evidence for an apparently single-step deprotection–cyclization reaction mediated by a benzoyl-localized  $n\pi^*$  triplet with  $\approx 11$  ns time constant in organic solvents like acetonitrile (CH<sub>3</sub>CN) and benzene. This agrees with the indirect results of facile quenching of the benzoin deprotection by conventional triplet quenchers.<sup>[2,3a,7]</sup> In contrast to this, the DMB deprotection is not quenched by triplet quenchers even in a neat quencher such as piperylene. Based on this evidence, diverse singlet character pathways proceeding via various reactive intermediates (Scheme 1) have been proposed in the literature, and the triplet state of such as the DMB ester, which was found to be long-lived ( $>10^{-6}$  s lifetime) and having absorptions at  $\approx 340$  nm and  $\approx 420$  nm, has been considered to be nonreactive towards deprotection and cyclization.<sup>[5,12]</sup>

In general, three types of intermediates, including two cations (the cyclic cation **1** and carbocation **2**) and a biradical species **3**, have been considered to be important in previous mechanistic studies of the DMB photodeprotection and cyclization reactions. Cation **1** is speculated to be produced by either 1) a C–X bond rupture accompanied by a ring-opening of a strained bicyclic oxetane intermediate, which results from an intramolecular Paterno–Büchi cycloaddition (Scheme 1, pathway a),<sup>[7]</sup> or 2) a C–X heterolytic cleavage of an intramolecular exciplex formed by charge transfer (CT) from the dimethoxybenzylic ring to the carbonyl  $n\pi^*$  singlet state (pathway b).<sup>[5]</sup> In this case, the cyclization product, 2-phenyl-5,7-dimethoxybenzofuran (DMBF), was considered to be formed from a subsequent H<sup>+</sup> elimination of the cation **1** intermediate. Results from a nanosecond laser flash photolysis (LFP) study by Wan and co-workers on a series of DMB esters led them to propose intermediate **1** to be assigned to a transient species with a  $\lambda_{\text{max}}$  absorption at  $\approx 480$  nm.<sup>[5]</sup> From the observation of a time-resolution (10 ns) limited formation and the  $\approx 1$   $\mu$ s lifetime of this species, it was suggested that a stepwise mechanism, with a quick deprotection (rate  $>10^8$  s<sup>-1</sup>) followed by a relatively slow DMBF formation (rate  $\approx 10^6$  s<sup>-1</sup>) for DMB esters in CH<sub>3</sub>CN, may occur.<sup>[5]</sup>

The cation **2** intermediate, formed either by 1) a direct heterolytic cleavage of the C–X bond or 2) a homolytic cleavage followed by an electron transfer in the radical pair, has been taken as the most likely intermediate to mediate not only the deprotection and cyclization processes in non-polar or polar aprotic solvents, but also to account for the additional solvolysis reaction that takes place in water or largely water-containing solvents.<sup>[3a]</sup> The involvement of a homolytic character for the C–X cleavage is disfavored by the absence of decarboxylation products observed after photolysis of DMB pivalate.<sup>[5]</sup> This lack of decarboxylation products, together with results from recent fs-TA kinetic experiments carried out by Pirrung, Simon, and co-workers, led to the proposal of an alternative stepwise mechanism (Scheme 1, pathway c) with an ultrafast excited-state hetero-



Scheme 1. Deprotection and cyclization pathways proposed in previous mechanistic studies of DMB compounds.

lytic deprotection cleavage (rate  $>10^{13} \text{ s}^{-1}$ ), giving intermediate **2** as a precursor (with a rate of  $\approx 10^{11} \text{ s}^{-1}$ ) to the cyclic **1** intermediate, which then undergoes deprotonation to yield DMBF.<sup>[3f]</sup>

Distinct from the above-mentioned pathways a, b, and c in Scheme 1, Chan and co-workers suggested that a biradical intermediate **3** is formed from a radical-based addition of the excited carbonyl oxygen to the substituted benzylic ring, to be the first reactive intermediate in the photodeprotection of a water soluble DMB acetate.<sup>[6]</sup> Upon the formation of intermediate **3**, acetoxy migration, followed by re-aromatization or nucleophilic attack by water at the benzylic carbon accounts for the cyclization (pathway d) in  $\text{CH}_3\text{CN}$  or the modest extent of extra solvolysis in water, respectively. A more recent fs-TA study by Wirz and co-workers on DMB acetate and fluoride led to another proposed mechanism (pathway e), which suggests that intermediate **3** is a precursor to cation **1**, with a  $\approx 2\text{--}3$  ns deprotection time constant for the two compounds in  $\text{CH}_3\text{CN}$ .<sup>[12]</sup> Within this model, similarly to pathways a, b, and c, the cyclization proceeds by the subsequent deprotonation of cation **1**. In this work, intermediate **3** was attributed to an fs-TA band that has  $\lambda_{\text{max}}$  at  $\approx 360$  nm and is formed with a time constant of  $\approx 20$  ps.

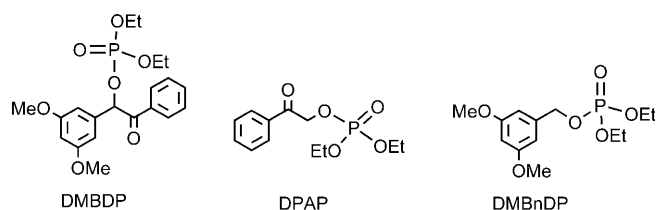
DMB is a bichromophoric system containing a benzoyl (Bz) chromophore and a 3',5'-dimethoxybenzyl (DMBn) chromophore. Among the previously proposed pathways, the cation **1** species appears to be a common intermediate attributed to the transient product of the heterolytic deprotection, and at the same time the immediate precursor to the formation of the cyclization product DMBF. The differences in the various proposed assignments of the penultimate precursor that leads to intermediate **1** originate from different views on the fundamental issue of which chromo-

phore, Bz or DMBn, plays the predominate role in the excited-state processes. This is because the locally excited process of both chromophores has been expected to display distinct excited states or transient species with different reactivities towards deprotection and cyclization. For example, the precursors of cation **1** (Scheme 1) suggested in pathways a (oxetane), b (exciplex), and d/e (biradical) were all based on a Bz-localized excitation and the consideration of a mainly radical-associated reactivity of the singlet  $n\pi^*$  excited state.<sup>[5,6,7,12]</sup> On the other hand, the attribution of cation **2** in pathway c rests on the primary role played by an excited state of the DMBn moiety, in that the 3,5-dimethoxy substitution on the benzylic ring can greatly enhance heterolytic cleavage at the benzylic carbon (e.g., through Zimmerman's *meta* effect), leading to rapid formation of the associated cation.<sup>[3a,f,8]</sup>

There are, however, difficulties for both kinds of basic conjectures to fully justify the very high efficiency of the DMB deprotection and reactivity of the involved excited state. For instance, in the case of the Bz-dominated excited reaction, it is known that electronic excitation of the Bz moiety typically causes rapid intersystem crossing (ISC), with time constants of  $\approx 2\text{--}3$  ps and giving a close to unit yield of a triplet state.<sup>[15–20]</sup> Therefore, it is unclear 1) how a  $\approx 20$  ps process, like that ascribed to give the biradical **3** intermediate, can compete efficiently with the ISC process to account for the high yield of the DMBF product, and 2) why the derived triplet is nonreactive (triplet energy transfer from Bz to DMBn is forbidden from an energy consideration), whereas the Bz-localized  $n\pi^*$  triplet, as revealed in the parent benzoin system, has been proven to be very reactive in giving rapid ( $\approx 10^8 \text{ s}^{-1}$  rate) deprotection–cyclization.<sup>[13a]</sup> As for the mechanisms associated with the DMBn chromophore, considering that the DMB photodeprotection

depends only slightly on excitation wavelength ( $\lambda_{\text{exc}}$ ) and shows a better efficiency with  $\lambda_{\text{exc}} > 300 \text{ nm}$ ,<sup>[3,5,7,8]</sup> it is not clear how the *meta* effect can operate efficiently: within the picture of localized photoexcitation, apparently only the Bz group could possibly be excited electronically at these wavelengths,<sup>[5,7,8,12]</sup> and the singlet energy transfer from the Bz chromophore to the DMBn chromophore is energetically forbidden.<sup>[5,21]</sup> Besides this, the previous mechanisms also have difficulties in their kinetic aspects in accommodating the observed subtle dependence of the DMB deprotection and cyclization efficiency on the leaving group and solvent polarity (except water).<sup>[3a,f,5,8,12]</sup> For example, according to the latest suggested pathway e, the heterolytic  $X^-$  elimination from radical **3** was assigned as a key reaction step in  $\text{CH}_3\text{CN}$ .<sup>[12]</sup> However, this would suggest that the deprotection rate, and hence the efficiency of the deprotection, would be substantially affected by the leaving group lability and solvent properties,<sup>[15a,b,22]</sup> which is not confirmed by experimental data. Additionally, the unusually high deprotection rate ( $\approx 10^{13} \text{ s}^{-1}$ ) proposed for pathway c<sup>[3f]</sup> has had little explicit evidence for similar extremely fast and efficient analogous reactions in the literature for this kind of mechanism. The preceding uncertainties suggest that more experimental characterization of the reaction intermediates and their properties is needed to understand the DMB deprotection and cyclization pathway more fully.

In this paper, a combined fs-TA and ns-TR<sup>3</sup> study on a typical DMB-caged compound, that is, DMB diethyl phosphate (DMBDP), in  $\text{CH}_3\text{CN}$  is reported. To elucidate the origin of the substitution effect and to explore the electronic character and reactivity of the DMBDP excited state (such as how and at which stage this may be influenced by interaction between the Bz and DMBz moieties), we have also performed a parallel fs-TA study on two model compounds, diethyl phosphate acetophenone (DPAP) and 3',5'-dimethoxybenzyl diethyl phosphate (DMBnDP).



The DPAP and DMBnDP compounds were synthesized to serve as reference systems to provide a spectral and dynamical characterization of the excited-state processes initiated by the individual electronic excitation of the Bz and DMBn chromophores, respectively. These time-resolved studies, combined with steady-state photochemistry measurements and related theoretical calculations, provide evidence for a novel *concerted* deprotection–cyclization mechanism, which bypasses the commonly referred to intermediate **1**, and which has a time constant for the DMBDP cyclization determined as  $\approx 1 \text{ ns}$ . Comparison of the results ob-

tained for DMBDP with those for DPAP and DMBnDP indicates that electronic interaction between the Bz and DMBn moieties plays a decisive role from the moment of photoexcitation, leading to a peculiar series of transient states and intermediates that constitute a distinct pathway for DMBDP deprotection and cyclization compared to systems in which this interaction is not present, such as DPAP, DMBnDP, and the parent benzoin-caged diethyl phosphate (BDP).

## Results

**Steady-state study:** Figure 1 shows the change in the UV spectra of DMBDP upon 266 nm photolysis in  $\text{CH}_3\text{CN}$  recorded after a series of defined periods of irradiation. Clear-

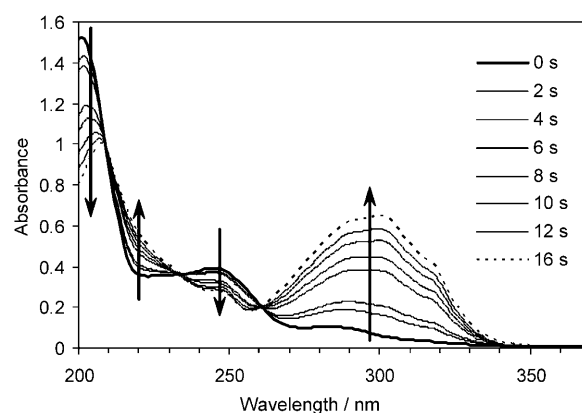


Figure 1. Change in the UV spectrum of DMBDP in  $\text{CH}_3\text{CN}$  with increasing 266 nm photolysis recorded prior to irradiation (0 s), and after 2, 4, 6, 8, 10, 12, and 16 s of exposure to laser irradiation.

ly, with an increase of the photolysis time, the DMBDP absorption (the 0 s time spectrum in Figure 1) transforms gradually into a different spectrum (the 16 s time spectrum in Figure 1), which is characteristic of an absorption spectrum due to the DMBF photoproduct.<sup>[3,7,8]</sup> The smooth spectral transformation is accompanied by the appearance of three well-defined isobestic points at  $\approx 208$ ,  $234$ , and  $\approx 262 \text{ nm}$ , indicating that there is direct photoinduced conversion of DMBDP into DMBF, as described in Equation (1). Using the absorption extinction coefficient reported for DMBF in ethanol ( $\epsilon_{310\text{nm}} = 27480 \text{ M}^{-1} \text{ cm}^{-1}$ )<sup>[3a]</sup> and assuming the same value in  $\text{CH}_3\text{CN}$ , the quantum yield of DMBF formation was estimated to be  $\approx 0.62 \pm 0.1$ ,<sup>[13c]</sup> close to the values reported in the literature for DMB acetate.<sup>[7a]</sup>

To better understand the influence of the dimethoxy substitution, and to assess the possible interaction between the Bz and DMBn moieties in the Franck–Condon region of photoexcitation, Figure 2 displays a comparison of the steady-state UV absorption spectra of DMBDP, DMBnDP, and DPAP in  $\text{CH}_3\text{CN}$ . As expected, the DPAP spectrum closely resembles the reported absorption spectrum of

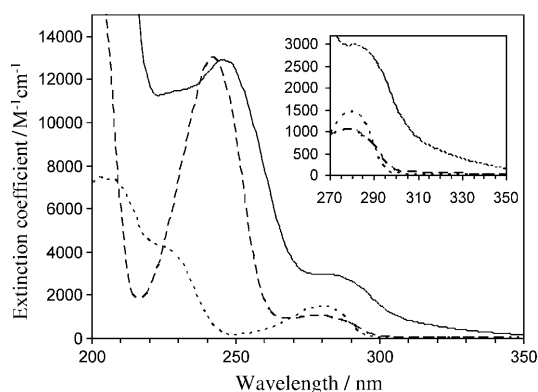


Figure 2. UV absorption spectra of DMBDP (solid line), DPAP (dashed line), and DMBnDP (dotted line), in  $\text{CH}_3\text{CN}$ . The inset shows enlarged spectra for the weak absorption in the  $\approx 270$  to 350 nm wavelength range.

AP,<sup>[3a,16,19,20,23]</sup> indicating that light absorption is accounted for by the common Bz chromophore, and that an analogous pattern of electronic transitions is involved in the photoexcitation of DPAP and AP. From the known spectral attribution of AP and related aromatic carbonyls,<sup>[16,19,20,23]</sup> the strong DPAP absorption band of  $\lambda_{\text{max}} \approx 240$  nm ( $\epsilon \approx 1.3 \times 10^4 \text{ M}^{-1} \text{ cm}^{-1}$ ) can be ascribed to the allowed  $\pi\pi^*$  transition ( $L_a$ ,  $S_3$ ) of the phenyl ring, the relatively weaker band at  $\approx 260$ –300 nm ( $\epsilon_{280\text{nm}} \approx 1.1 \times 10^3 \text{ M}^{-1} \text{ cm}^{-1}$ ) to the less-allowed ring  $\pi\pi^*$  ( $L_b$ ,  $S_2$ ) transition, and the very weak but characteristic absorption at  $\approx 300$ –350 nm ( $\epsilon_{310\text{nm}} \approx 80 \text{ M}^{-1} \text{ cm}^{-1}$ , see Figure 1, inset) to the carbonyl  $n\pi^*$  ( $S_1$ ) transition. The DMBnDP spectrum is typical of the absorption spectra of benzene and related Bn compounds.<sup>[21,25]</sup> However, compared to the corresponding bands of these Bn derivatives, the lowest energy  $\pi\pi^*$  absorption in DMBnDP ( $\lambda_{\text{max}} \approx 280$  nm,  $\epsilon \approx 1.4 \times 10^3 \text{ M}^{-1} \text{ cm}^{-1}$ ) is redshifted significantly, and has a marked increase in its oscillator strength. This agrees with the general trend of the spectral changes in this  $\pi\pi^*$  absorption as induced by the ring substitution,<sup>[21]</sup> and reflects that the ring 3,5-substitution by the strongly electron-donating methoxy groups leads to a substantial energy stabilization of the correlated excited state relative to the ground state ( $S_0$ ). It is noted that the transition energy of this DMBnDP absorption is comparable to the  $L_b$   $\pi\pi^*$  absorption in DPAP. However, DMBnDP shows no discernible absorption at wavelengths  $> 300$  nm. From the above results and the fact that the diethyl phosphate (DP) leaving group absorbs only in the far UV region, the spectra of DPAP and DMBnDP can each be taken as benchmark absorption spectra for the Bz and DMBn chromophores, respectively.

The UV/Vis absorption of DMBDP at wavelengths  $> 240$  nm appears to be similar to that of DPAP. However, close examination shows that, besides the strong  $\approx 240$  nm band, which appears to be fairly comparable in the two compounds, the two lower energy bands of DMBDP at the  $\approx 270$ –300 and 300–350 nm regions clearly display stronger oscillator strengths than their DPAP counterparts. As the DMBDP spectrum cannot be decomposed into the individual absorptions due to the Bz and DMBn chromophores, it is

possible that the absorptions may arise from electronic transitions with noticeably different character, and are likely to be due to excitations that involve both the Bz and DMBn moieties. Indeed, our TDDFT computational results obtained from the optimized structure of the ground  $S_0$  state of DMBDP (see Figure 1S and Table 1S in the Supporting Information) indicate that the absorption of the two lower energy bands are due to electronic transitions correlated with both the Bz and DMBn moieties. For example, the  $\approx 270$ –300 nm absorption arises from localized  $\pi\pi^*$  transitions at either the Bz or DMBn rings, with sizeable contributions due to an interchromophore  $\pi\pi^*$  transition from the DMBn to Bz moiety. For the 300–350 nm band, besides the Bz-localized  $n\pi^*$  transition, participation also comes from extensive delocalized transitions from the bonding orbital of DMBn to the antibonding orbital of Bz and the carbonyl group. The involvement of these CT types of transitions in the FC excitation, which is not seen clearly in many other  $\alpha$ -keto phototriggers,<sup>[1,2,13,15,24,26,27]</sup> may present an important aspect for the ensuing unique photodeprotection properties of the DMB PRPG. This is verified by the fs-TA and ns-TR<sup>3</sup> measurements described in the rest of the paper.

**Femtosecond transient absorption (fs-TA) spectroscopy:** To help unravel the excited-state processes for the DMBDP photodeprotection and to elucidate the roles played by the Bz and DMBn moieties in the DMBDP photodeprotection, comparative fs-TA measurements were carried out for DMBDP, DPAP, and DMBnDP in  $\text{CH}_3\text{CN}$ . The results obtained for DPAP and DMBnDP are presented first, because they provide necessary reference information for the interpretation of the DMBDP excited states and for assessment of the various earlier proposed deprotection pathways. In addition, the significance of the excited-state properties, reactivity, and dynamics of these two compounds by themselves renders these femtosecond time-resolved data, which have not been available in the literature, interesting in their own right. For example, DPAP can be regarded as a phenacyl-caged compound.<sup>[1,24]</sup> For this type of PRPG, a previous LFP study on the ns- $\mu\text{s}$  timescale revealed a triplet hydrogen abstraction pathway for the photodeprotection of the phenacyl acetate.<sup>[24]</sup> However, the earlier stage excited states that exist before several nanoseconds have remained uncharacterized. DMBnDP, on the other hand, provides a good example of a DMBn-caged compound.<sup>[14,28,29]</sup> Since the pioneering work of Zimmerman<sup>[14,29]</sup> in showing the *meta*-effect and the remarkable facile photosolvolysis reactivity for di-*meta*-methoxy-substituted benzylic systems, the DMBn chromophore has been frequently employed in the design of practical PRPGs, and this has attracted much interest in the excited-state behavior of DMBn compounds.<sup>[28,30]</sup> Although many studies have provided valuable information for the excited-state dissociation of DMBn systems,<sup>[14,28–30]</sup> it has remained unclear as to the fundamental mode, homolytic versus heterolytic breaking, of the bond cleavage; the rate of the bond breaking has also remained unknown. Our results here for DMBnDP provide, to the

best of our knowledge, the first direct determination of these parameters, which are of general interest for DMBn systems.

**Femtosecond TA measurements for DPAP:** Figure 3 shows representative fs-TA spectra recorded for DPAP at time delays of up to 5000 ps after 267 nm excitation, which direct-

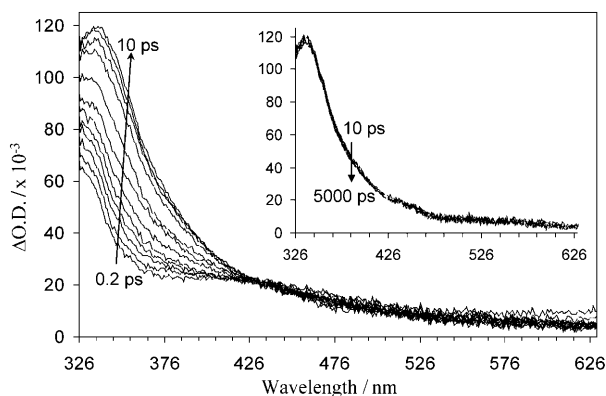


Figure 3. Fs-transient absorption spectra of DPAP obtained by 267 nm excitation in  $\text{CH}_3\text{CN}$  at early picosecond times of 0.2, 0.3, 0.6, 0.8, 1, 1.25, 1.75, 2.5, 4.5, 6, 10 ps, and later picosecond times (inset) of 10, 20, 100, 500, 1000, and 5000 ps.

ly populates the strong  $\pi\pi^*$  ( $L_a$ ) state of DPAP. The temporal evolution of the spectra displays rapid conversion within  $\approx 10$  ps from the early spectrum (the 0.2 ps spectrum, absorbing at  $< \approx 340$  nm wavelength region) into a spectrum (the 10 ps spectrum) that shows a relatively strong absorption with its  $\lambda_{\text{max}}$  at  $\approx 350$  nm. This 350 nm absorption displays little decay at later times (see Figure 3, inset). The kinetics for the spectral changes of the TA spectra were followed using the 345 nm wavelength, and Figure 4 displays the TA time profile at  $\approx 345$  nm together with a single exponential fitting convolved with the instrumental response function (IRF) of the TA measurements. The fitting results

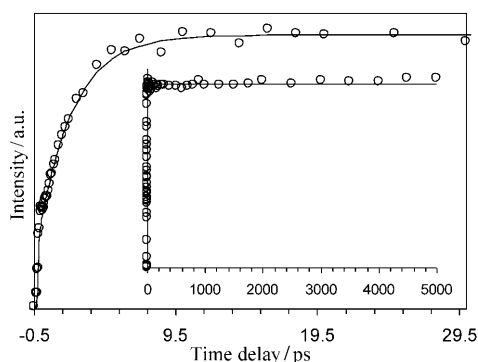


Figure 4. Time dependence of the DPAP transient absorption spectra in  $\text{CH}_3\text{CN}$  (shown in Figure 3) at  $\approx 345$  nm at early and later (inset) picosecond times. The solid lines indicate the kinetics fitting to the experimental data points using an exponential function convolved with the IRF.

in a  $\approx 2.5$  ps time constant for the rising component observed at early picosecond times.

The  $\approx 350$  nm absorption spectrum closely resembles the triplet absorption spectrum of AP in the same solvent,<sup>[17,18]</sup> and is also consistent with the triplet absorption of phenacyl group compounds, as reported in previous LFP studies on phenacyl esters.<sup>[24]</sup> Therefore, this spectrum can be confidently attributed to the Bz-localized triplet ( $T_1$ ) state of DPAP. From this, it is straightforward to attribute the  $\approx 2.5$  ps process to an ISC that leads to rapid conversion of the system from the initially photoexcited singlet to a triplet state. The rapid ISC agrees with the high triplet yield generally observed for related aromatic carbonyls.<sup>[15–20]</sup> Given the extremely rapid nature of the internal conversions (IC) from  $S_3$  to  $S_1$ , we tentatively attribute the very early (0.2 ps) spectrum to the  $S_1$   $\pi\pi^*$  state. The persistence of the  $\approx 350$  nm triplet spectrum at late picosecond times is consistent with the lower reactivity of the  $T_1$  state in the inert  $\text{CH}_3\text{CN}$  solvent (in terms of the hydrogen abstraction reaction), in which the triplet decay is determined mainly by a ns– $\mu\text{s}$  diffusion-controlled oxygen quenching process.<sup>[15,24,31]</sup>

The TA results for DPAP reveal a photophysical transformation [Eq. (2)] to account for the early time deactivation associated with the Bz-localized photoexcitation. The data provide characteristic absorption spectra for the Bz-localized  $S_1$  (the 0.2 ps spectrum) and  $T_1$  (spectrum of 10 ps or later) states.



**Fs-TA measurements for DMBnDP:** Figure 5 displays the temporal evolution of the fs-TA spectra obtained after 267 nm photoexcitation of DMBnDP in  $\text{CH}_3\text{CN}$ . The 267 nm excitation takes the population of the system to the  $\pi\pi^*$  excited state, and the initial 0.2 ps spectrum can be ascribed to the  $S_1$   $\pi\pi^*$  state, the spectrum of which is broad and apparently has two  $\lambda_{\text{max}}$  at  $\approx 370$  nm and 510 nm. It is clear from Figure 5 that, immediately after photoexcitation,

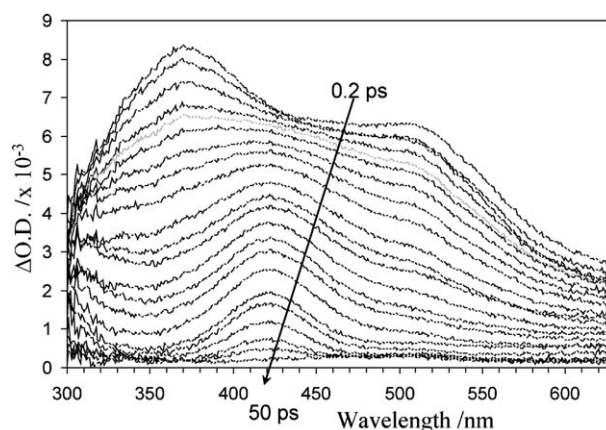


Figure 5. Fs-transient absorption spectra of DMBnDP obtained after 267 nm excitation in  $\text{CH}_3\text{CN}$  at delay times of 0.2, 0.4, 0.6, 0.8, 1, 1.2, 1.4, 1.6, 2, 2.25, 3, 3.5, 4.5, 7, 8.5, 12, 18, 25, and 50 ps.

the  $S_1$  spectrum decays quickly into a distinctly different profile (the spectrum of  $\approx 5$  ps or later), which features a single absorption with  $\lambda_{\text{max}}$  of  $\approx 425$  nm; this  $\approx 425$  nm spectrum then decays and disappears on the  $\approx 50$  ps timescale. Figure 6 shows the TA time profiles at the representative

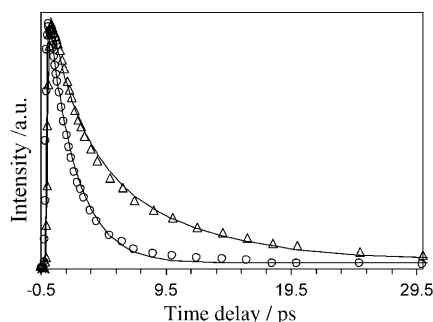


Figure 6. Normalized time dependences of the DMBnDP transient absorption spectra in  $\text{CH}_3\text{CN}$  (shown in Figure 5) at  $\approx 370$  nm ( $\circ$ ) and  $\approx 425$  nm ( $\triangle$ ). The solid lines indicate kinetics fitting to the experimental data points using exponential functions convolved with the IRF.

wavelengths of  $\approx 370$  and  $\approx 425$  nm. Fitting of this profile by using single (the  $\approx 370$  nm data) or double (the  $\approx 425$  nm data) exponential function(s) convolved with the IRF gives a common time constant of  $\approx 2.1$  ps from both the data sets for the early  $S_1$  decay, and a  $\approx 7.7$  ps time constant (from the  $\approx 425$  nm profile) for the later disappearance of the  $\approx 425$  nm spectrum.

Of the many kinds of substituted benzyl compounds, the di-*meta*-methoxy-substituted systems are among those having the lowest fluorescence quantum yield ( $\phi_f$  of  $\approx 10^{-3}$  order of magnitude) in polar solvents.<sup>[28,30]</sup> The  $\approx 2.1$  ps  $S_1$  decay time observed here provides a direct determination of the  $S_1$  deactivation rate, and explains these low  $\phi_f$  values. This very short  $S_1$  lifetime indicates a very high efficiency for the nonradiative event(s) that depopulates the  $S_1$  state. Our data above suggest that as the  $S_1$  decays, the system is converted into a short-lived ( $\approx 7.7$  ps) intermediate that is responsible for the  $\approx 425$  nm spectra.

To help identify this intermediate and the underlying pathway leading to the  $\approx 425$  nm species, we consider three possible  $S_1$  deactivation channels proposed previously in the literature:<sup>[14,28–30]</sup> 1) ISC to a triplet state, 2) C–O bond homolysis to give a radical pair  $\text{DMBn}^{\cdot}\text{DP}$ , and 3) C–O bond heterolysis to produce an ion pair  $\text{DMBn}^+\text{DP}^-$ . Process 1 appears rather unlikely, because although the triplet of some benzyl esters have been reported to absorb at  $\approx 400$  nm (close to the observed absorption),<sup>[28c]</sup> the triplet is expected to have a much longer lifetime in the ns– $\mu\text{s}$  range due to its known nonreactivity towards an excited-state bond cleavage.<sup>[28–30]</sup> Process 2 also seems unlikely, due to the fact that the radical species, which has DMBn as a chromophore, is expected to display an absorption in the  $\approx 320$ – $340$  nm region, similar to absorption spectra observed previously for various benzyl radicals.<sup>[32,33,34–36]</sup> Process 3 emerges

as a plausible attribution for the observed process and the associated intermediate, and is supported by several pieces of evidence, such as the fact that: 1) many benzyl cations have been found to absorb in the  $\approx 410$ – $450$  nm wavelength range,<sup>[32,33,37]</sup> and 2) the importance of the direct excited-state C–X (X = leaving group) heterolytic cleavage has been implicated in many earlier studies to interpret the noticeably enhanced yield of ion-derived products observed for di-*meta*-methoxy/substituted benzyl esters and phosphates.<sup>[14,28,30,38]</sup> Further relevance to this end is that CASSCF theoretical studies by Zimmerman<sup>[14]</sup> indicate an evident energy preference for the  $S_1$  heterolysis relative to homolysis, and suggest the presence of an easily accessible conical intersection between the  $S_1$  and  $S_0$  potential surfaces to offer an efficient avenue for the excited-state ion pair to decay radiationlessly to the  $S_0$  surface. Based on the preceding results, we ascribe the  $\approx 425$  nm signal to the  $\text{DMBn}^+$  ion, which is formed by direct C–O heterolysis of the  $S_1$  state. The observed rapid decay ( $\approx 7.7$  ps) of the  $\approx 425$  nm signal can be readily explained by the high reactivity of the nascent  $\text{DMBn}^+$  cation. Upon formation, this kind of cation is subject to extremely efficient reactions, including the in-cage ion-pair recombination to return to the original DMBnDP molecule, and the solvolytic addition reaction.<sup>[28,30,32,33,38]</sup> Although the specific partitioning between these two channels may depend on various factors, the very high efficiency of the recombination pathway has been demonstrated by  $^{18}\text{O}$  scrambling experiments on closely related benzylic compounds, as reported by Givens and co-workers.<sup>[38]</sup> From these results, and given the lower reactivity of the  $\text{CH}_3\text{CN}$  solvent towards solvolytic addition,<sup>[39]</sup> the very fast decay of  $\text{DMBn}^+$  can be mainly attributed to the ion pair collapse leading to re-formation of the reactant substrate.

It is worth noting that the results here for DMBnDP in  $\text{CH}_3\text{CN}$  represent the first direct spectral and dynamical characterization of the singlet excited state and associated heterolysis for benzylic and ring-substituted benzylic compounds. This observation lends strong experimental support to Zimmerman's *meta* effect,<sup>[14,29]</sup> in that the *meta*-methoxy substitution favors strongly the excited singlet state heterolysis. This also offers an explicit example indicating that the ionic products observed for DMBnDP, and probably for some DMBn esters as well, in solvents such as alcohols and water<sup>[28,30]</sup> could also be due to ionic intermediates (the cation) that originates from the *direct* heterolysis pathway, rather than the *indirect* pathway of charge transfer preceded by homolysis. However, given that the mode of the excited-state bond rupture (homolysis versus heterolysis) can be affected sensitively by diverse factors, such as properties of the leaving group, the polarity and solvation capability of the solvent medium, ring substitution, and so on,<sup>[28,30,32,33]</sup> further study is required to establish whether, or to what extent, the direct excited-state heterolysis mechanism can be applied to other related benzyl compounds. Nonetheless, for the purpose of the work reported here, the spectral and kinetic information acquired for the  $S_1$  and  $\text{DMBn}^+$  ion from

DMBnDP provides the needed reference benchmark for a discussion of the nature and dynamical transformation of the DMBDP excited state, which is examined in the next section.

*Fs-TA measurement for DM-BDP:* The fs-TA spectra recorded for DMBDP over a range of time intervals following excitation at 267 nm reveals the presence of a series of consecutive spectral changes in the timescale up to 6 ns. To show the temporal evolution of the spectra clearly in different time regimes, the spectra obtained at several typical time intervals are displayed separately in Figure 7. A 3D overview of all the spectra is given in the Supporting Information (Figure S2).

Immediately after photoexcitation (Figure 7a), the spectrum shows evolution from a profile featuring a broad absorption with apparently two  $\lambda_{\max}$  at  $\approx 335$  and 450 nm (the 0.6 ps spectrum) to a different profile also exhibiting a broad absorption, but with apparently one  $\lambda_{\max}$  at  $\approx 345$  nm (the 3.5 ps spectrum). This spectral change is accompanied by three isosbestic points at  $\approx 350$ , 430, and 530 nm, suggesting the occurrence of a state-to-state conversion which is denoted temporally as **A**  $\rightarrow$  **B**, with **A** related to the very early time ( $< 0.6$  ps) spectra and **B** to the somewhat later 3.4 or 4.0 ps spectra. From Figure 7b and c it can be seen that, at the time interval from 4 to  $\approx 50$  ps, the **B**-related spectra decay, and there is simultaneous growth of a new band with  $\lambda_{\max}$  at  $\approx 370$  nm, assumed to arise from a species denoted as **C**<sub>370</sub>. From 50 to 1500 ps, the **C**<sub>370</sub> (the 50 ps spectrum is characteristic of the **C**<sub>370</sub> species) species spectrum decays again, and at the expense of this decay, two new bands with  $\lambda_{\max}$  at  $\approx 320$  and 480 nm appear due to another species. From their simultaneous growth, the  $\approx 320$  and  $\approx 480$  nm bands can be considered to arise either from a common species or from two individual ones. These two bands are denoted as being due to the **D**<sub>320</sub> and **D**<sub>480</sub> species, respectively. The observation of two sets of isosbestic points associated with the two spectral transformations in the two different time regimes (Figure 7b and c) indicates there are direct dynamic conversions taking place, and mother-to-daughter relationships between the correlated species. After 1500 ps (Figure 7d), the **C**<sub>370</sub>- and **D**<sub>480</sub>-associated bands both exhibit an intensity decrease, but with different dynamics, whereas the **D**<sub>320</sub>-related band shows relatively little change in intensity.

The kinetics for the above-mentioned spectral transformations, and possibly other intermediates involved in these transformations, can be traced by following the TA time profiles at typical absorption wavelengths for the species of interest. Figure 8 displays the temporal changes of the TA spectra at the  $\approx 375$ ,  $\approx 495$ , and  $\approx 420$  nm wavelengths, at different ranges of time intervals. The two-phase growth exhibited by the  $\approx 375$  nm profile at early times ( $\leq 15$  ps, inset in Figure 8a) reflects the dynamics for the **A**  $\rightarrow$  **B** and **B**  $\rightarrow$  **C**<sub>370</sub> transformations. The subsequent intensity decay and corresponding growth of the  $\approx 375$  and  $\approx 495$  nm profiles, respectively, at timescales up to 700 ps (Figure 8a) contain the dynamics for the **C**<sub>370</sub>  $\rightarrow$  **D**<sub>480</sub> (+**D**<sub>320</sub>) conversion. The later

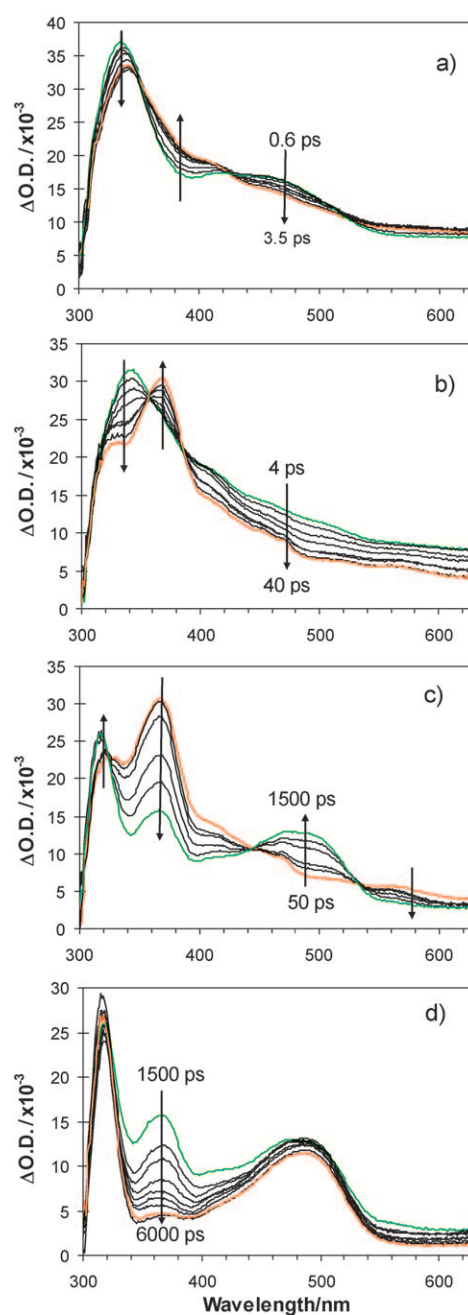


Figure 7. Fs-transient absorption spectra of DMBDP obtained subsequent to 267 nm excitation in CH<sub>3</sub>CN at delay time intervals from a) 0.6 to 3.5 ps, b) 4 to 40 ps, c) 50 to 1500 ps, and d) 1500 to 6000 ps.

time TA decay (Figure 8b) is wavelength dependent. The TA time profile at some wavelengths, such as  $\approx 420$  and  $\approx 340$  nm, and also those associated with the **D**<sub>480</sub> species at  $\approx 495$  nm, display much slower decays than that of the profile at  $\approx 375$  nm.

Global multiexponential fittings of the TA profiles at various wavelengths including those in Figure 8 (e.g., solid lines in Figure 8) give time constants of  $\approx 1.7$ ,  $\approx 14$ , and  $\approx 1050$  ps for the first three transformation steps, respectively. As for the ensuing later time dynamics, the least square fitting of

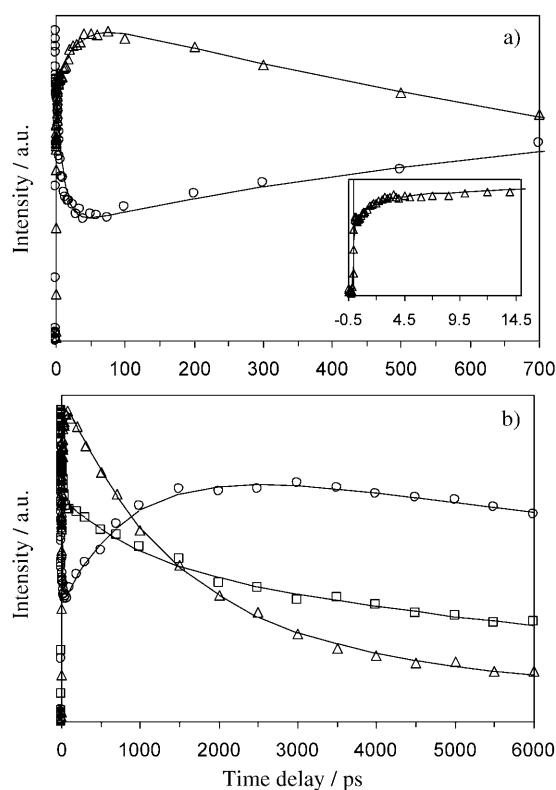


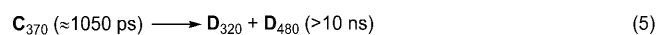
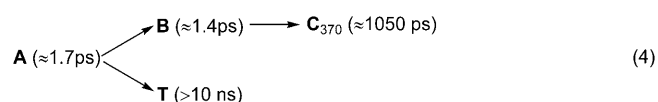
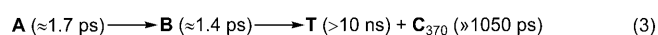
Figure 8. Normalized time profiles of the DMBDP transient absorption in  $\text{CH}_3\text{CN}$  (Figure 7) at  $\approx 375$  nm ( $\Delta$ ),  $\approx 495$  nm ( $\circ$ ), and  $420$  nm ( $\square$ ). The solid lines are from fitting of the experimental data by multiexponential functions convolved with the IRF. The inset in a) shows the two-phase grow-in kinetics as indicated by the  $375$  nm time profile at early delay times (see text for details).

the  $\approx 375$  and  $\approx 420$  nm time profiles requires the inclusion of an additional fourth component of  $\geq 10$  ns time constant, with a relatively higher weighted contribution for the  $\approx 420$  nm wavelength than the  $\approx 375$  nm profile. In the same way, the slow decay of the  $\mathbf{D}_{480}$  related profiles can be described by a time constant of  $\geq 10$  ns.

It is noted that these long-lived spectral components have also been observed on a microsecond timescale by previous LFP measurements on DMB esters in  $\text{CH}_3\text{CN}$ .<sup>[5]</sup> The  $\mathbf{D}_{480}$  associated component evidently corresponds to the  $\lambda_{\text{max}}$  of  $480$  nm ( $\approx 1 \mu\text{s}$  lifetime) LFP absorption, corresponding to the cation  $\mathbf{1}$  of previous studies (see Scheme 1). The  $\geq 10$  ns absorption at wavelengths around  $\approx 420$  and  $\approx 340$  nm is consistent with the triplet-state absorption reported for DMB acetate,<sup>[5,12]</sup> and thus can be associated with the triplet state ( $\mathbf{T}$ ) of DMBDP. The broad nature of the TA spectra at early times (Figure 7a–c) together with the rather slow decay of the  $\mathbf{T}$  state makes it difficult to track the precise timing for its formation. However, the spectral evolution and wavelength-dependent decay in Figure 8b indicates that the  $\mathbf{T}$  and  $\mathbf{C}_{370}$  species coexist, and both contribute to the relatively early spectra shown in Figure 7b and c, but with the  $\lambda_{\text{max}}$   $370$  nm absorption contributed predominantly from the  $\mathbf{C}_{370}$  species, and the absorption at  $\approx 420$  and  $\approx 340$  nm more

from the  $\mathbf{T}$  species. These two species may display overlapped absorptions to a different extent at some other wavelengths. Similarly to the case here, the TA spectra at a comparable time regime ( $< 50$  ps) from the joint contributions due to the  $\mathbf{T}$  and a  $\lambda_{\text{max}}$   $360$  nm species (assigned to the biradical  $\mathbf{3}$  in path e of Scheme 1) have also been reported in a fs-TA study on DMB acetate in  $\text{CH}_3\text{CN}$ .<sup>[12]</sup>

The preceding kinetic analysis can be used to develop a scheme for the dynamical transformations observed in the TA spectra, and to account for the excited-state events occurring after photoexcitation of DMBDP [see Eqns. (3)–(5)]. Among the various properties of the transient species included in the scheme, the TA character determined for the very early stage  $\mathbf{A}$  and  $\mathbf{B}$  states and the explicit identification of the  $\mathbf{D}_{320}$  species provide important new insights for evaluating the different deprotection and cyclization pathways (Scheme 1) proposed in previous studies.



As mentioned in the introduction section, the DMBDP reaction pathways suggested earlier are based on local excitation of either the Bz or DMBn moieties, and governed by the corresponding transient states/species, that is, mainly the carbonyl localized  $\text{S}_1$  state in the case of the Bz moiety predominant process versus the heterolytic cation  $\mathbf{2}$  involved in the DMBn sub-chromophore predominant process (Scheme 1). These states or species were speculated in the literature to be extremely short-lived, and present only at very early times after photoexcitation.<sup>[3a,f,5–7,12]</sup> The validity of these hypotheses would be demonstrated by the expectation that the initial and early-stage excited states of photoexcited DMBDP would display, to a certain extent, a spectral and dynamical character comparable to the excited states or species associated with either the Bz or the DMBn chromophore. Our aforementioned TA data on DPAP and DMBnDP supplies benchmark results for making such an assessment. Comparing the early time ( $< 5$  ps) TA spectra and the temporal evolution of photoexcited DMBDP (Figure 7a) with those of DPAP (Figure 3) and DMBnDP (Figure 5) reveals, however, a distinctly different character of the DMBDP spectra from either chromophore benchmark (DPAP and DMBnDP) or a combination of them. For example, the initial Bz-localized  $\text{S}_1$  state has an absorption  $\lambda_{\text{max}}$  at  $< 340$  nm, and then transforms by  $\approx 2.5$  ps ISC into the Bz-localized  $\text{T}_1$  featured by the  $\lambda_{\text{max}}$   $\approx 350$  nm band, with little absorption at wavelengths  $> 450$  nm. This contrasts with the DMBDP results in that the  $\mathbf{A}$  and  $\mathbf{B}$  states both ex-

hibit broad absorptions throughout the visible region. The lack of a general common feature in the spectral profiles is also seen clearly when comparing the DMBDP **A**- and **B**-state TA spectra with those of the  $S_1$  and  $DMBn^+$  species of  $DMBnDP$ . It also appears unlikely that the DMBDP excited states could be described as an overlapped contribution from the excited states/species associated with the individual Bz and  $DMBn$  locally excited processes. This is because it turns out to be difficult to decompose the early DMBDP spectra into a weighted combination of the corresponding DPAP and  $DMBnDP$  spectra, despite our many attempts to do so.

This observation of little similarity in the early TA spectra of the DMBDP excited state with those expected by the locally excited Bz and/or  $DMBn$  corroborates the UV/Vis absorption (Figure 2) and TDDFT results on DMBDP. These together suggest that, for DMBDP, the electronic interaction between the two moieties leads not only to the delocalized  $S_0$  to  $S_n$  absorption transition(s), but also to the involvement of discrete excited states and ensuing species, which could not be accounted for only on the basis of locally excited chromophores.

As for the  $D_{320}$  species, we note that our observation of the simultaneous dynamical growth of the correlated  $\lambda_{320}$  absorption with the  $\lambda_{480}$  absorption (Figure 7c) has not been reported in the literature to the best of our knowledge. This could be due to the different time and spectral windows used in this work from those of previous studies,<sup>[3f,5,12]</sup> and may also relate to the presence of the promptly formed, but long-lived, triplet-state absorption at a similar wavelength region.<sup>[5,12]</sup> Considering the fact that the absorption of the DMBF final product [Eq. (1)] extends to this wavelength region and is much stronger than the absorption of the DMBDP reactant (Figure 1), it turns out to be quite possible that the  $\lambda_{320}$  absorption (Figure 7c and d) may arise from a transient DMBF product resulting from the deprotection and cyclization of the photoexcited DMBDP. The drastic TA drop at the blue edge of the  $\lambda_{320}$  absorption (Figure 7) is due to the limited spectral detection window of the present TA measurements. Making use of the ability of resonance Raman spectroscopy to enhance selectively the Raman spectra of species that are in resonance with the electronic absorption of that species,<sup>[13,15]</sup> our resonance Raman (RR) and ns-TR<sup>3</sup> results described below provide unequivocal evidence for the attribution of the  $D_{320}$  species to the transient DMBF. This constitutes a key piece of information, which leads us to a dramatically revised picture for the DMBDP deprotection and cyclization reaction.

**Nanosecond time-resolved resonance Raman (ns-TR<sup>3</sup>) spectroscopy of DMBDP:** The ns-TR<sup>3</sup> measurements were designed and performed to explore and ascertain the identity of the  $D_{320}$  species observed in the TA spectra, as well as to determine the formation dynamics of the DMBF cyclization product for photoexcited DMBDP in  $CH_3CN$ . Using the UV/Vis absorptions of DMBF and DMBDP (Figure 1), pump and probe wavelengths of 240 and 299 nm, respective-

ly, were carefully chosen to facilitate the ns-TR<sup>3</sup> measurements. The 240 nm pump was selected due to the relatively strong absorption of the DMBDP reactant compared to the DMBF product at this wavelength. The 299 nm probe is close to the  $\lambda_{max}$  of the DMBF lowest energy absorption, and is also close to the  $D_{320}$  absorption observed in the TA spectra.

The ns-TR<sup>3</sup> spectra obtained with the 240 nm pump and 299 nm probe wavelengths at the indicated delay times are given in Figure 9. A 299 nm resonance Raman (RR) spec-

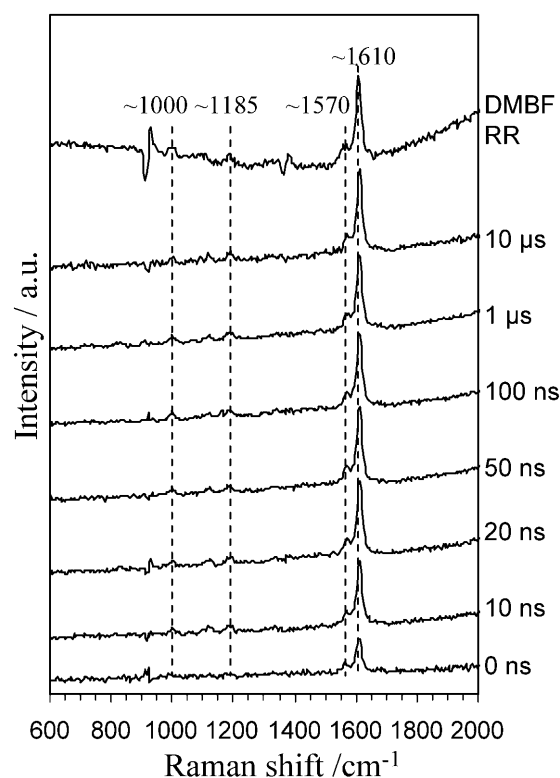


Figure 9. Nanosecond time-resolved resonance Raman spectra of DMBDP in  $CH_3CN$  obtained with 240 nm/299 nm pump/probe wavelengths at the indicated delay times. At the top is the resonance Raman spectrum of DMBF acquired with 299 nm excitation in  $CH_3CN$ .

trum from a synthesized authentic sample of DMBF acquired under the same conditions is also displayed in Figure 9, to allow comparison and to help identify the transient revealed in the ns-TR<sup>3</sup> spectra. The ns-TR<sup>3</sup> spectra of DMBDP in Figure 9 show an instant appearance of a series of features (mainly the strong  $\approx 1610$   $cm^{-1}$  feature and weak features at  $\approx 1570$ , 1180, and 1000  $cm^{-1}$ ) with their intensities reaching their maxima within the approximate time resolution of our ns-TR<sup>3</sup> measurement ( $\approx 10$  ns), and these intensities nearly constant after 10 ns (Figure 3S, Supporting Information). Comparison of these transient Raman spectra with the DMBF RR spectrum shows clearly that the vibrational features in the former are essentially identical to those of the latter. This offers explicit evidence for the assignment of the ns-TR<sup>3</sup> features to the DMBF product.

Taken together, the data in Figure 9 provide unambiguous evidence for a rapid yield of the DMBF product with a formation time of  $< 10$  ns. The constant ns-TR<sup>3</sup> signal level observed on the ns to  $\mu$ s timescale indicates there is little relevance of a long-lived species ( $> 10$  ns lifetime) in the DMBF product formation. To the best of our knowledge, the ns-TR<sup>3</sup> results here provide the first direct time-resolved monitoring of the cyclization reaction for DMP PRPGs.

Incorporating these results with the temporal evolution scheme observed based on the fs-TA data leads us to associate the TA observed **D**<sub>320</sub> species with the DMBF product revealed in the resonance Raman measurements. With this assignment and the dynamic result in Equation (5), it is considered that the DMBDP photocyclization takes place from the **C**<sub>370</sub> precursor and proceeds with a  $\approx 1050$  ps time constant, corresponding to a rate of  $\approx 10^9$  s<sup>-1</sup>. The **C**<sub>370</sub> species also serves as a common precursor to give the **D**<sub>480</sub> intermediate, a process which occurs competitively with the cyclization reaction. The cyclization pathway revealed here differs fundamentally from those proposed in the earlier studies not only in the ordering of reactive intermediates, but also in the dynamics of the reaction. The previously proposed pathways, although they have diverse descriptions for the very early time excited state/species, have a general consensus that the cyclization occurs with a  $\approx 10^6$  s<sup>-1</sup> rate and had the  $\lambda_{480}$  species (corresponding to **D**<sub>480</sub> here) as the precursor for the cyclization (Scheme 1).<sup>[3f,5-7,12]</sup>

## Discussion

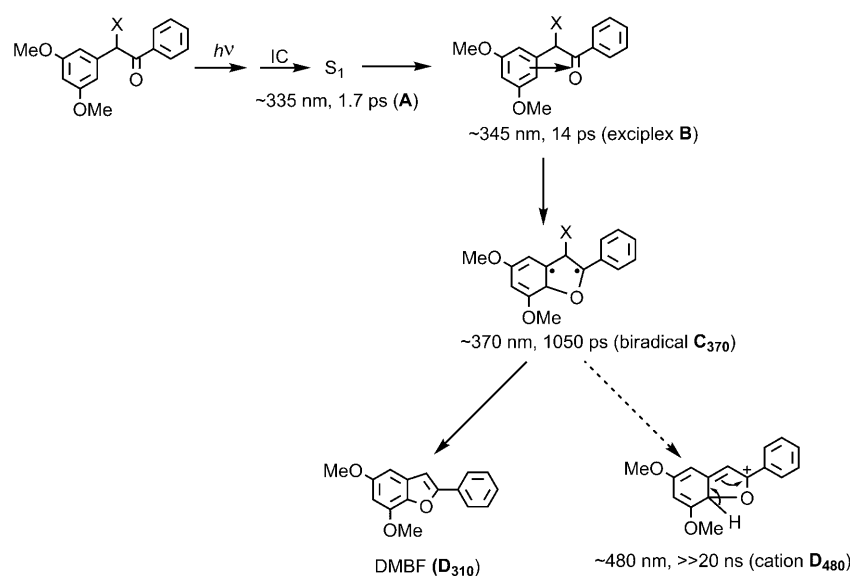
Understanding the nature of the series of photoinitiated transformations, as revealed in the TA data, and the make-up of the transient states and intermediates involved, is essential for elucidating the mechanistic details of the DMBDP photodeprotection and cyclization, and the underlying cause of the unusual di-*meta*-methoxy substitution effect. Comparison of the steady-state UV/Vis and time-resolved fs-TA results obtained for the target DMBDP and the two reference compounds DPAP and DMBnDP in CH<sub>3</sub>CN have revealed spectral and dynamical features of the target molecule that are distinctive from the reference systems. This indicates that the nature of the photoexcitation and subsequent excited-state events and dynamics for DMBDP are intrinsically different from those expected from local excitation of either the Bz or DMBn sub-chromophore. From this and the related TDDFT absorption, electronic-transition results, it is reasonable to consider that, for DMBDP, the electronic communication between the Bz and DMBn moieties upon and after photoexcitation may play a decisive role in accounting for the delocalized excitation, the involvement of the exclusive series of transient states and species, and, more importantly, the explicit outcome of the DMBDP photolysis. As implied by the complex and rich photochemistry exhibited by the diverse substituted benzoinyl compounds in terms of giving substantially varied yields of the cyclization and some other products,<sup>[1-3,5-8,12]</sup>

the operation and way of operation of this electronic interaction could depend critically on the pattern and composition of the substitution on both the Bz and benzylic phenyl rings. Extensive previous work on this aspect, based mainly on product analysis, found consistently that the di-*meta*-methoxybenzylic substitution represents the optimal chromophore design in offering a clean and highly efficient photodeprotection and cyclization reaction.<sup>[3,7,8]</sup> This may imply further that the incorporation of this particular pattern of substitution can induce an appropriate electronic modulation to promote the needed delocalized excitation, and at the same time facilitate the particular set of excited-state steps to bring about a highly efficient photoliberation reaction. To substantiate this, it appears relevant to make a comparison of the excited-state behavior and photochemical outcome for DMBDP and the parental benzoin-caged diethyl phosphate (BDP).

**Substitution effect of the benzoinyl chromophore:** Previous studies on BDP<sup>[2a,13a]</sup> show that photolysis of this compound in CH<sub>3</sub>CN leads to the formation of a Bz-localized S<sub>1</sub>, which converts by a  $\approx 2$ –3 ps ISC to a Bz-localized T<sub>1</sub> state, from which then proceeds, with  $\approx 11$  ns time constant, an apparently single-step phosphate liberation and cyclization to yield the BF product. It is consistent to this end that the spectral features and the ISC dynamics of the BDP S<sub>1</sub> and T<sub>1</sub> states closely resemble the corresponding results shown here for DPAP. Unlike the triplet-natured pathway of BDP, our observation that photolysis of DMBDP leads to the DMBF product being formed on a timescale ( $\approx 1$  ns) much faster than the decay ( $\geq 10$  ns) of its T state provides direct evidence to exclude the T state as a reactive precursor to the DMBDP cyclization. This affords an explicit explanation for the previously reported lack of triplet quenching effect, and on the other hand implicates a singlet-character channel for the DMBDP photodeprotection and cyclization, which is in accordance with most of the earlier proposed mechanisms<sup>[3a,f,5-7,12]</sup> with regard to the excited-state multiplicity of the DMBDP photoliberation. It is interesting to note that the determined timing of DMBDP cyclization is more than one order of magnitude faster than the BDP cyclization. This may contribute to the much higher efficiency of the DMBDP compared to the BDP reaction. The nonreactivity of the DMBDP T, and the low T yield as can be inferred from the high efficiency of the competing singlet pathway, contrast sharply with the primary role of the BDP T state in the BDP photoliberation reaction. The origin of this could also be the peculiar electronic interaction between the Bz and the DMBn sub-chromophores in DMBDP, which renders its triplet having intrinsically different features from those of the Bz-localized triplet of BDP. Considering the modest role of the T state in the DMBDP excited-state deactivation and its minor relevance to the deprotection reaction, this state will not be included in the following sections.

**Possible assignments and mechanistic pathway for the DMBDP photodeprotection and cyclization:** Although our

fs-TA data obtained for DMBDP provide clear evidence for the participation of a series of dynamically correlated transient species in the excited-state deactivation and cleavage reaction, it appears difficult to make straightforward assignments to these intermediates based solely on the broad, and in some cases overlapped, absorption features. However, referring to the valuable insight presented in previous DMB mechanistic studies,<sup>[3a,f,5–8,12]</sup> and taking into account the electronic and spectral features reported in the literature for some related compounds and intermediates, we consider the following attributions to each of the observed transient species to be rather reasonable, and form a basis to suggest an alternative mechanistic picture (Scheme 2) for DMBX (X = leaving group) deprotection and cyclization in CH<sub>3</sub>CN. It is envisaged that this single mechanism may apply also to the deprotection reaction taking place in other polar aprotic solvents, and also nonpolar solvents.



Scheme 2. Deactivation and photodeprotection and cyclization pathway of DMBDP in CH<sub>3</sub>CN suggested from the time-resolved spectra presented here and other results in the literature.

The 267 nm photoexcitation of DMBDP takes the system to an upper singlet ( $S_{n>1}$ ) excited state (Figure 2). The generally prompt IC is expected to lead the  $S_{n>1}$  population to relax promptly to the  $S_1$  state. We thus relate the  $S_1$  state to the denoted **A** state of the fs-TA spectra. This state corresponds to the directly accessed singlet excited state when using a  $>340$  nm excitation, the desirable and frequently used excitation wavelength in many of the previous studies.<sup>[3a,f,5–8]</sup> In view of the electron-donating and accepting capacity of the Bz and DMBn moieties,<sup>[3f,5,7,8]</sup> respectively, and a probably enhanced ability induced by the electronic excitation,<sup>[5,12,40,41]</sup> we tentatively associate the observed **B** state to the CT exciplex suggested by Wan and co-workers (in pathway b of Scheme 1). It is pertinent to this point that many of the previous studies on the excited states of (aro-

matic) ketones bearing an electron-rich  $\alpha$ - or  $\beta$ -aryl group have suggested involvement of an exciplex or a complex formed by CT from the aryl to the carbonyl to account for the markedly efficient excited-state quenching and reactions.<sup>[42–47]</sup> The observed very rapid nature ( $\approx 1.7$  ps) of the  $S_1$  **A** to exciplex **B** transformation implies the process is essentially a barrierless excited-state conversion, likely to be associated with small structural changes. It is worth noting that the timescale for this conversion in DMBDP is close to that of the DPAP  $S_1$  to  $T_1$  ISC ( $\approx 2.5$  ps) and the cleavage of  $S_1$  to DMBn<sup>+</sup> for DMBnDP ( $\approx 2.1$  ps). However, the distinctly different character of the spectral profile revealed by our TA data (Figures 3, 5, and 7) indicates clearly the participation of entirely different species for these dynamically similar processes. This underlines the importance of the TA broad-band capability in differentiating transient intermediates involved in excited-state events of comparable dynamics.

For the  $C_{370}$  intermediate, the formation time ( $\approx 14$  ps) determined here for DMBDP is comparable to that of the  $\lambda_{\max}$  360 nm species reported for DMB acetate and fluoride ( $\approx 17$  ps) by Wirz and co-workers.<sup>[12]</sup> Since this intermediate is the immediate reactive precursor giving the cyclization reaction [Eq. (5)], the observations that 1) its formation dynamics show little dependence on the basicity of the leaving group,<sup>[5,12]</sup> and 2) the cyclization yield is affected only modestly by solvent polarity and is favored slightly in nonpolar over polar solvents,<sup>[3a,f,5,8,7,12]</sup> lend strong support to its attribution as the biradical-natured intermediate suggested by Wirz and co-workers<sup>[12]</sup> and Chan and co-workers<sup>[6]</sup> (species **3** in path-

ways d and e in Scheme 1). Corroborating further this ascription, as well as the **B** exciplex to the  $C_{370}$  biradical conversion, there have been many precedents in the literature involving a quick transformation from an early CT exciplex to a biradical precursor to account for photocyclization reactions of aromatic ketones.<sup>[40,43,46,48–50]</sup> We note, however, that the previous studies by Wirz and Chan have provided no specification as to the nature of the electronic state for the  $C_{370}$  biradical.<sup>[12]</sup> The  $\approx 1$  ns lifetime of this species for DMBDP implies that it would correspond to a fairly well-defined local minimum of the related potential hypersurface. Our DFT calculations, intending to locate such a configuration in the singlet ground-state surface by considering either a *syn* or *anti* arrangement of the phosphate group relative to the liable *ortho*-hydrogen of the DMBn subgroup, lead in-

evitably to structures with fission of the C–O bond connecting the phosphate and the DMB cage (see Figures 4S and 5S, and Tables 2S and 3S in the Supporting Information for details of the optimized structures). From this, we conjecture that, instead of being a ground-state species, the biradical may still reside on the singlet excited-state surface, and is formed by addition of the carbonyl oxygen (O) to the *ortho*-carbon (C) of the benzylic ring. For a singlet-natured species, such a bonding process is spin-allowed and,<sup>[31]</sup> in the particular case of the CT exciplex of DMBDP, the bonding could be further facilitated by the intramolecular CT interaction between the DMBn-associated donor and the Bz-associated acceptor.<sup>[3a,f,5,7,8,12,14,29]</sup> The rapid dynamics of biradical formation ( $\approx 14$  ps) suggests the addition reaction is a fairly feasible excited-state process. Given the largely non-planar conformation (with a nearly orthogonal relative orientation of the Bz and DMBn ring planes, and the far-beyond-bonding separation of the associated C and O atoms) of the DMBDP ground state (see Figure 1S and Table 1S in the Supporting Information) and the probably similar structure of the exciplex precursor, it is possible that the O–C addition is largely an entropy-controlled process that requires substantial conformational rearrangement, such as alignment to a certain extent of the two ring systems and synchronous motion of the connecting carbon atoms, and so forth. This parallels the widely recognized aspect that the kinetics of many intramolecular photocyclizations are subject to strong conformational and stereoelectronic control.<sup>[42,43,45,51]</sup> In nonpolar and polar aprotic solvents, such as CH<sub>3</sub>CN, the flexible construction of the DMBDP molecule renders the needed conformation easily achievable, and this may contribute to the rapid dynamics and high efficiency of the O–C addition.

Our fs-TA and ns-TR<sup>3</sup> data on DMBDP show that, upon decay of the C<sub>370</sub> biradical (Scheme 2), the system may convert either directly to the DMBF product or to the D<sub>480</sub> intermediate. With the biradical attribution of the C<sub>370</sub> species, the former channel presents a concerted HX elimination–cyclization pathway for DMBDP photodeprotection. As this channel works as the major pathway leading to the DMBF product, the efficiency of the cyclization reaction would be determined largely by the branching ratio of this to the competing D<sub>480</sub> formation. The generally high DMBF yield, as reported consistently in previous studies, indicates a modest yield of D<sub>480</sub>. From this and the rather strong  $\lambda_{480}$  absorption, as suggested in the fs-TA spectra (Figure 7), a D<sub>480</sub> species with fairly large molar absorptivity may be implied. Our TDDFT calculations for the structurally optimized cation **1** (Scheme 1) reveals a strong absorption with an oscillator strength of  $\approx 0.45$  at a wavelength of  $\approx 440$  nm (see Figure 6S and Table 4S in the Supporting Information for details). This appears to support the attribution of D<sub>480</sub> to the cation **1**, a connection originally proposed by Wan and co-workers.<sup>[5]</sup> With this assignment, the C<sub>370</sub> biradical to D<sub>480</sub> cation conversion can be considered as an X<sup>−</sup> elimination channel, similar to that suggested by Wirz and co-workers in terms of this particular step (path e in Scheme 1).<sup>[12]</sup> Howev-

er, in contrast to most of the literature work in considering the cation **1** as a key precursor to the subsequent rate-determining H<sup>+</sup> elimination to give the DMBF cyclization product, our ns-TR<sup>3</sup> data here indicate explicitly that this cation is largely irrelevant to the cyclization, and that formation of this species could represent a competing but energy-wasting channel, probably leading mainly to re-formation of the reactant substrate or some other minor byproduct(s) with low efficiency towards the cyclization reaction. As for the previously suggested ultrafast ( $\approx 10^{13}$  s<sup>−1</sup> rate) heterolysis cleavage pathway, which gives the cation **2** as a reactive intermediate (path c in Scheme 1),<sup>[3f]</sup> the distinct difference in the early time (< 1 ps) TA spectra of DMBDP from those of DMBnDP, and the apparent lack in the DMBDP spectra of the characteristic  $\lambda_{\text{max}} \approx 420$  cation absorption as exhibited by the closely related DMBn<sup>+</sup>, suggests that such a process, if present, could play only a minor role in DMBDP photolysis in CH<sub>3</sub>CN.

From the above description of the assignments and dynamical conversions of the various intermediates, a pathway for DMBDP deprotection can be constructed (Scheme 2). After photoexcitation, the S<sub>1</sub> transforms rapidly ( $\approx 1.7$  ps) into a CT exciplex (**B**), which then undergoes intramolecular C–O addition with  $\approx 14$  ps time constant to yield the *product-determining* intermediate, that is, the singlet excited biradical C<sub>370</sub>. Bifurcation of the biradical decay leads primarily to a concerted HX elimination, and to a much lesser extent to an X<sup>−</sup> elimination, with the former pathway producing the DMBF product directly, while the latter results in the mainly *non-product-forming* D<sub>480</sub> cation.

It is interesting to note that, although our ascription of the C<sub>370</sub> biradical to a singlet excited species implies a singlet excited-state calculation (which is very difficult to perform for this large system with two chromophores) is needed to elucidate the detailed conformation and energy properties of this species in giving the deprotection reaction and any accompanied byproduct, our preliminary DFT results on the ground state of this species, which are computationally easier and more tractable (see Figure 4S–6S and Tables 2S–4S in the Supporting Information), appear to contain useful information for understanding the mode of the proposed concerted HX elimination and the formation of the D<sub>480</sub> cation. On the one hand, the observation that the *syn*-arrangement fragments into phosphoric acid and a structure analogous to the DMBF product (Figure 4Sa and Table 2 Sa) is consistent with an intramolecular character *syn* elimination of HX in accounting for the concerted deprotection–cyclization process. It is likely that for the operation of this elimination mode, the phosphate group may act as an intramolecular base to help in removing the liable hydrogen. On the other hand, the result that the *anti*-arrangement fragments into the phosphate anion (X<sup>−</sup>) and a counterpart cation, as indicated by the calculated charge distribution (Figure 5Sa and Table 3S in the Supporting Information), may suggest formation following such a conformation of a contact ion pair. Given the same chemical constitution and the general resemblance in the charge and structural ar-

range of the counterpart cation to that of the  $\mathbf{D}_{480}$  cation (Figure 6S and Table 4S in the Supporting Information), it is conceivable that the  $\mathbf{D}_{480}$  cation may arise from the charge separation of the contact ion pair and correspond to the counterpart cation involved in the ion pair. This *anti*-structure-associated ion-pair formation and charge separation may constitute a pathway giving the competing  $X^-$  elimination of the  $\mathbf{C}_{370}$  biradical. Because the efficiency of the ion-pair formation and the charge separation depends critically on the polarity property of the solvent,<sup>[15a,b,22,31,39]</sup> a higher yield of the  $\mathbf{D}_{480}$  cation in a polar solvent is expected within this assignment than in a nonpolar solvent. In fact, an absence of the absorption due to the  $\mathbf{D}_{480}$  cation has been reported for photolysis of DMB-caged acetate in cyclohexane (a nonpolar solvent),<sup>[12]</sup> in contrast to the clear involvement of such an absorption as observed for the same system in  $\text{CH}_3\text{CN}$  (a polar solvent).<sup>[5,12]</sup>

The mechanistic scenario proposed here (Scheme 2) reconciles nicely with several important experimental observations reported for DMB deprotection in aprotic polar and nonpolar solvents. Within this model, the decay rate of the biradical  $\mathbf{C}_{370}$ , which equals the sum of the rates of the HX ( $k_{\text{HX}}$ ) and the  $X^-$  ( $k_{X^-}$ ) eliminations, serves as a measure of the overall rate ( $\approx 1 \times 10^8 \text{ s}^{-1}$ ) for liberation of the leaving group; the concerted HX elimination is the rate-determining step for the deprotection and cyclization with its efficiency determined by the ratio of the  $k_{\text{HX}}$  to the overall rate. Assuming the excited-state nature of the radical  $\mathbf{C}_{370}$ , HX elimination from this species to generate the extensively conjugated ground-state DMBF would appear to be a highly exothermic and kinetically feasible reaction, likely to be associated with an early transition state.<sup>[31]</sup> The proposed intramolecular nature of the HX elimination implies the reaction requires little assistance from the surrounding medium. These attributes appear to corroborate the general high efficiency of the deprotection and cyclization and the fact that this reaction is largely independent of the polarity property of the solvent (except in the case of water).<sup>[3a,f,5,7,8,12]</sup> The suggestion of the leaving group working as an intramolecular base to facilitate the concerted *syn* elimination accommodates nicely the fact that the kinetic decay of the biradical  $\mathbf{C}_{370}$  depends modestly on the leaving group involved in the reaction. With the increase in lability of the leaving group from fluoride to acetate to diethyl phosphate, the biradical decay rate increases, so the decay time constants become smaller, to range from  $\approx 3 \text{ ns}$  for fluoride to  $\approx 2 \text{ ns}$  for acetate<sup>[12]</sup> and further to  $\approx 1 \text{ ns}$ , as revealed here for the phosphate leaving group. In addition, previous studies have found a slightly lower cyclization efficiency of DMBX in aprotic polar than nonpolar solvents. For example, the relative cyclization efficiency of DMB acetate was reported to be  $\approx 86\%$  in  $\text{CH}_3\text{CN}$  and  $\approx 95\%$  in cyclohexane.<sup>[12]</sup> From our perspective, this can be rationalized in terms of a lower involvement in the nonpolar than the polar solvent of the  $X^-$  elimination process relative to the HX elimination process in accounting for the biradical decay. This is as expected according to the *anti*-associated  $X^-$  elimination pathway

proposed in the preceding paragraph. It is possible that the lack of the  $\mathbf{D}_{480}$  cation for the photolysis of DMB acetate in cyclohexane<sup>[12]</sup> may indicate a complete suppression of the  $X^-$  elimination channel, thus rendering the HX elimination an overwhelmingly predominant excited-state reaction in the nonpolar environment.

The photodeprotection mechanism of DMB photolysis in aqueous solution is of particular interest due to the biological relevance of the aqueous medium. However, like many other useful  $\alpha$ -keto PRPGs,<sup>[1,2,13,15,26,27]</sup> DMB photolysis in water or largely water-containing solvent gives different products from those in polar aprotic or nonpolar solvents.<sup>[6,12]</sup> Photolysis of DMB acetate, fluoride,<sup>[12]</sup> and a water-soluble DMB acetate<sup>[6]</sup> in largely or wholly water solutions has revealed that, as for the liberation of the leaving groups, the cyclization is prevented in a substantial fraction ( $\approx 30\%$ ) of photoproduct and, at the expense of this, there is formation of a second solvolytic water addition product of the corresponding benzoin. A similar solvent dependence of product distribution has also been reported for photolysis of parent benzoin compounds in aqueous versus aprotic solvents.<sup>[2a,13a]</sup> The appearance of the extra benzoin product at the expense of BF for BDP photolysis in aqueous solution has been found to be caused by the additional involvement of a kinetically competitive heterolytic dissociation to bifurcate the triplet deprotection–cyclization and to result in the formation of a triplet  $\alpha$ -ketocation from the common precursor of the Bz-localized triplet.<sup>[2a,13a]</sup> In spite of the intrinsically different features of the DMBDP photodeprotection from that of BDP, as illustrated in the preceding sections, the observation of an analogous photosolvolytic product in DMBDP may imply that its benzylic carbon must be accessible to nucleophilic attachment by water at a certain stage along the photolysis pathway. In parallel to the photosolvolytic pathway of the parent BDP, and also to take into account the high dissociation and solvation capacity of solvent water molecules in promoting rapid heterolytic cleavage,<sup>[2a,13a,15a,b,17,26,39]</sup> it appears rather reasonable to consider the inclusion of a similar cation species, the cation **2** proposed by Pirrung and co-workers,<sup>[3a,f]</sup> as the transient precursor to the solvolysis product from photolysis of the DMB compounds in the predominantly water environment. Further study is underway to detect directly the relevant transient species, and to explore the specific photodeprotection pathway of DMB compounds in aqueous solutions.

## Conclusion

A combined fs-TA and ns-TR<sup>3</sup> study has been performed to characterize the reactive intermediates and to detect directly the dynamics and pathways for DMBDP photodeprotection and cyclization in  $\text{CH}_3\text{CN}$ . To assess the molecular cause of the unusual di-*meta*-methoxy substituent effect, parallel fs-TA measurements have been carried out on two reference compounds, DPAP and DMBnDP, in the same solvent. Comparison of the UV/Vis and fs-TA data obtained for

these compounds and relevant TDDFT results reveals distinctively different spectral and dynamical features for DMBDP from those of the reference systems. The results suggest that, for DMBDP, electronic interaction between the two sub-chromophores plays a governing role in accounting for the involvement of a peculiar set of transient states and species and the discrete deactivation and deprotection pathways. By directly monitoring the temporal generation of the DMBF product, the DMBDP cyclization time constant was determined to be  $\approx 1$  ns in  $\text{CH}_3\text{CN}$ . This indicates explicitly that the long-lived species of the **T** state and the commonly discussed  $\lambda_{\text{max}}$  480 nm cation play only a minor role in the DMBDP photodeprotection and cyclization. In contrast to the previously suggested singlet *stepwise* deprotection and cyclization pathway, a revised singlet *concerted* deprotection–cyclization mechanism was proposed. This mechanism includes a rapid  $\approx 1.7$  ps conversion of the initial excited state into a CT exciplex that transforms with  $\approx 14$  ps time constant to a singlet excited  $\lambda_{\text{max}}$  370 nm biradical, which acts as the key reactive precursor to the ensuing leaving group liberation and cyclization. The deprotection of the biradical proceeds with  $\approx 1$  ns time constant and is caused by competition between two different reactions, of which the concerted HDP elimination constitutes the predominant pathway leading directly to yield the DMBF final product, whereas the heterolytic  $\text{DP}^-$  elimination that gives the  $\lambda_{\text{max}}$  480 nm cation works only as a minor pathway, bearing little relevance to the cyclization reaction. This work contributes important new insights for an improved mechanistic description of DMB photodeprotection, and helps give a better understanding of the structure/reactivity relationship of the DMB PRPG.

## Experimental Section

**Materials:** DMBDP, DPAP, and DMBnDP were synthesized following the methods described in the Supporting Information. The identity and purity of the samples were confirmed by NMR and UV absorption spectroscopy, and mass spectrometry. The details of the NMR characterization of the synthesized samples are given in the Supporting Information. DMBF was synthesized according to the photolysis method described in the literature,<sup>[2a]</sup> but replacing BDP with DMBDP. Spectroscopic grade  $\text{CH}_3\text{CN}$  was used as the solvent for all the steady-state and time-resolved experiments.

**UV absorption measurement:** The UV absorption spectra from the dilute sample solution in  $\text{CH}_3\text{CN}$  ( $\approx 1$  mM concentration) were measured using a Perkin–Elmer Lambda 19 UV/Vis spectrometer. The molar extinction coefficients ( $\text{M}^{-1}\text{cm}^{-1}$ ) were calculated based on the Beer–Lambert law.

**Photochemistry experiments:** The proceeding of the deprotection reaction initiated by photolysis of DMBDP in  $\text{CH}_3\text{CN}$  was monitored by measuring spectral change in UV absorption of a DMBDP sample solution (in a 1 cm UV cell) after various periods of exposure to an unfocused 266 nm laser line ( $\approx 1$  mJ). The 266 nm light is from the fourth harmonic of a nanosecond Nd:YAG Q-switch laser.

**Femtosecond transient absorption (fs-TA) experiments:** The fs-TA measurements were performed by using a commercial femtosecond Ti:Sapphire regenerative amplifier laser system. Details of the TA experimental setup are described in references [13, 15]. For the present measurements, sample solutions were excited by a 267 nm pump beam (the third har-

monic of 800 nm, the regenerative amplifier fundamental) and probed by a white light continuum probe beam produced from a rotating  $\text{CaF}_2$  plate pumped by the fundamental laser pulses (800 nm). The pump and probe laser beam spot sizes at the sample were about 200 and 100  $\mu\text{m}$ , respectively. The signals were focused into a monochromator and detected by a liquid- $\text{N}_2$ -cooled CCD. The time delay between the pump and probe pulse was controlled by an optical delay line, and the time resolution of the measurement was  $\approx 200$  fs. The TA measurements were carried out, respectively, for DMBDP, DPAP, and DMBnDP in  $\text{CH}_3\text{CN}$  at a sample concentration of  $\approx 1$  mM.

**Ns-time-resolved resonance Raman (ns-TR<sup>3</sup>) experiments:** The ns-TR<sup>3</sup> spectra presented here for DMBDP in  $\text{CH}_3\text{CN}$  were obtained by using the experimental apparatus and methods described previously.<sup>[13, 15]</sup> Briefly, the sample solution was pumped by a 240 nm excitation wavelength and probed by a 299 nm wavelength light. The pump and probe pulse were provided, respectively, by the first anti-Stokes and Stokes output from a  $\text{H}_2$  Raman shifter, each pumped by the fourth harmonic output (266 nm) of two individual Nd:YAG lasers. The time delay between the pump and probe pulses was controlled electronically by a pulse generator, and the time resolution of these measurements was  $\approx 10$  ns. The pump and probe laser beams were lightly focused onto a flowing sample solution and the Raman scattering was collected through a backscattering configuration and detected by a liquid- $\text{N}_2$ -cooled CCD. The resonance Raman spectrum of DMBF in  $\text{CH}_3\text{CN}$  was acquired by using a 299 nm excitation wavelength, with the signal collection configuration similar to that of the ns-TR<sup>3</sup> measurements. Sample concentrations for these Raman experiments were  $\approx 1$  mM. The wavenumber shifts of the resonance Raman spectra were calibrated using the known  $\text{CH}_3\text{CN}$  solvent Raman bands, and the ns-TR<sup>3</sup> spectra presented were obtained by subtracting an appropriately scaled probe-before-pump spectrum from the corresponding pump-probe spectrum.

**Density functional theoretical (DFT) calculations:** The TDDFT calculations were carried out employing the Gaussian 03 program suite.<sup>[52]</sup> The calculations were performed to obtain transition energies and oscillation strengths of electronic transitions of the species of interest. For each of the systems, the calculation was performed based on the optimized structure of the studied system obtained firstly by DFT geometry optimization computation. To find out the optimized structure(s) for the singlet ground state of the DMBDP biradical, the energy optimization calculation was first done for the triplet ground state of this species. This gave two optimized conformations, corresponding to diastereomers with the diethyl phosphate group being *syn* and *anti* relative to the liable *ortho*-hydrogen in the DMBn sub-group (see Figures 4Sb and 5Sb and Tables 2Sb and 3Sb in the Supporting Information). These geometries were then used as initial conformations to acquire the corresponding optimized structures for the singlet ground state of the biradical, as shown in Figures 4Sa, 5Sa, and Tables 2Sa and 3a in the Supporting Information. All of the calculations were performed using the B3LYP method with a 6–31G\* basis set.

## Acknowledgements

This research was carried out in the Ultrafast Laser Facility at the University of Hong Kong and supported by grants from the Research Grants Council of Hong Kong (HKU 1/01C and HKU 7039/07P) to D.L.P. and (PolyU 7029/06P and PolyU 7029/07P) to W.M.K. D.L.P. thanks the Croucher Foundation for the Award of a Senior Research Fellowship and the University of Hong Kong for the Outstanding Researcher Award.

[1] R. S. Givens, L. W. Kueper, *Chem. Rev.* **1993**, *93*, 55–66.

[2] a) C. S. Rajesh, R. S. Givens, J. Wirz, *J. Am. Chem. Soc.* **2000**, *122*, 611–618; b) R. S. Givens, P. S. Athey, L. W. Kueper, B. Matuszewski, J. Y. Xue, *J. Am. Chem. Soc.* **1992**, *114*, 8708–8710; c) R. S. Givens, P. S. Athey, B. Matuszewski, L. W. Kueper, J. Y. Xue, T. Fister, *J. Am. Chem. Soc.* **1993**, *115*, 6001–6012.

- [3] a) M. C. Pirrung, L. Fallon, D. C. Lever, S. W. Shuey, *J. Org. Chem.* **1996**, *61*, 2129–2136; S. W. Shuey, *J. Org. Chem.* **1994**, *59*, 3890–3897; b) M. C. Pirrung, C. Y. Huang, *Tetrahedron Lett.* **1995**, *36*, 5883–5884; c) M. C. Pirrung, J. C. Bradley, *J. Org. Chem.* **1995**, *60*, 1116–1117; d) M. C. Pirrung, C. Bradley, *J. Org. Chem.* **1995**, *60*, 6270–6276; e) M. C. Pirrung, L. Fallon, D. C. Lever, S. W. Shuey, *J. Org. Chem.* **1996**, *61*, 2129–2136; f) M. C. Pirrung, T. Ye, Z. Zhuo; J. D. Simon, *Photochem. Photobiol.* **2006**, *82*, 1258–1264; J. D. Simon, *Photochem. Photobiol.* **2006**, *82*, 1258–1264.
- [4] J. M. Peach, A. J. Pratt, J. S. Snaith, *Tetrahedron* **1995**, *51*, 10013–10024.
- [5] Y. Shi, J. E. T. Corrie, P. Wan, *J. Org. Chem.* **1997**, *62*, 8278–8279.
- [6] R. S. Rock, S. I. Chan, *J. Am. Chem. Soc.* **1998**, *120*, 10766–10767.
- [7] a) J. C. Sheehan, R. M. Wilson, A. W. Oxford, *J. Am. Chem. Soc.* **1971**, *93*, 7222–7228; b) J. C. Sheehan, R. M. Wilson, *J. Am. Chem. Soc.* **1964**, *86*, 5277–5281.
- [8] J. F. Cameron, C. G. Wilson, J. M. J. Frechet, *J. Am. Chem. Soc.* **1996**, *118*, 12925–12937.
- [9] C. P. McCoy, C. Rooney, C. R. Edwards, D. S. Jones, S. P. Gorman, *J. Am. Chem. Soc.* **2007**, *129*, 9572–9573.
- [10] J. E. T. Corrie, D. R. J. Trentham, *Chem. Soc. Perkin Trans. 1* **1992**, 2409–2417.
- [11] a) R. S. Rock, S. I. Chan, *J. Org. Chem.* **1996**, *61*, 1526–1529; b) R. P.-Y. Chen, J. J.-T. Huang, H.-L. Chen, H. Jan, M. Velusamy, C.-T. Lee, W. Fann, R. W. Larsen, S. I. Chan, *Proc. Natl. Acad. Sci. USA* **2004**, *101*, 7203–7310; c) R. S. Rock, K. C. Hansen, R. W. Larsen, S. I. Chan, *Chem. Phys.* **2004**, *307*, 201–208.
- [12] H. Boudebous, B. Kosmrlj, B. Sket, J. Wirz, *J. Phys. Chem. A* **2007**, *111*, 2811–2813.
- [13] a) C. Ma, W. M. Kwok, Y. Du, D. L. Phillips, *Chem. Eur. J.* **2007**, *13*, 2290–2305; b) W. S. Chan, C. Ma, W. M. Kwok, P. Zuo, D. L. Phillips, *J. Phys. Chem. A* **2004**, *108*, 4047–4058; c) Y. Du, PhD. Thesis, University of Hong Kong **2007**.
- [14] a) H. E. Zimmerman, *J. Phys. Chem. A* **1998**, *102*, 5616–5621; b) H. E. Zimmerman, *J. Am. Chem. Soc.* **1995**, *117*, 8988–8991.
- [15] a) C. Ma, W. M. Kwok, W. S. Chan, P. Zuo, J. T. W. Kan, P. H. Toy, D. L. Phillips, *J. Am. Chem. Soc.* **2005**, *127*, 1463–1472; b) C. Ma, W. M. Kwok, W. S. Chan, Y. Du, J. T. W. Kan, P. H. Toy, D. L. Phillips, *J. Am. Chem. Soc.* **2006**, *128*, 2558–2570; c) W. S. Chan, C. Ma, W. M. Kwok, D. L. Phillips, *J. Phys. Chem. A* **2005**, *109*, 3454–3469; d) P. Zuo, C. Ma, W. M. Kwok, W. S. Chan, D. L. Phillips, *J. Org. Chem.* **2005**, *70*, 8661–8675; e) C. Ma, P. Zuo, W. M. Kwok, W. S. Chan, J. T. W. Kan, P. H. Toy, D. L. Phillips, *J. Org. Chem.* **2004**, *69*, 6641–6647; f) C. Ma, W. S. Chan, W. M. Kwok, P. Zuo, D. L. Phillips, *J. Phys. Chem. A* **2004**, *108*, 9264–9276.
- [16] a) D. R. Kearns, W. A. Case, *J. Am. Chem. Soc.* **1966**, *88*, 5087–5097; b) W. A. Case, D. R. Kearns, *J. Chem. Phys.* **1970**, *52*, 2175–2191.
- [17] M. B. Ledger, G. Porter, *J. Chem. Soc. Faraday Trans.* **1972**, *68*, 539–553.
- [18] H. Lutz, E. Breheret, L. Lindqvist, *J. Phys. Chem.* **1973**, *77*, 1758–1762.
- [19] P. M. Rentzepis, *Science* **1970**, *169*, 239–247.
- [20] P. J. Wagner, A. E. Kemppainen, H. N. Schott, *J. Am. Chem. Soc.* **1973**, *95*, 5604–5614.
- [21] M. Montalti, A. Credi, L. Prodi, M. T. Gandolfi, *Handbook of Photochemistry*, CRC Press, New York, **2006**.
- [22] a) M. Newcomb, J. H. Horner, P. O. Whitted, D. Crich, X. Huang, Q. Yao, H. Zipse, *J. Am. Chem. Soc.* **1999**, *121*, 10685–10694; b) J. H. Horner, E. Taxil, M. Newcomb, *J. Am. Chem. Soc.* **2002**, *124*, 5402–5410; c) P. O. Whitted, J. H. Horner, M. Newcomb, X. Huang, D. Crich, *Org. Lett.* **1999**, *1*, 153–156.
- [23] S. Dym, R. M. Hochstrasser, *J. Chem. Phys.* **1969**, *51*, 2458–2468.
- [24] A. Banerjee, D. E. Falvey, *J. Am. Chem. Soc.* **1998**, *120*, 2965–2966.
- [25] S. Tournon, M. A. El-Bayoumi, *J. Chem. Phys.* **1972**, *56*, 5128–5134.
- [26] P. G. Conrad, R. S. Givens, B. Hellrung, C. S. Rajesh, M. Ramseier, J. Wirz, *J. Am. Chem. Soc.* **2000**, *122*, 9346–9347.
- [27] a) K. Zhang, J. E. T. Corrie, V. R. N. Munasinghe, P. Wan, *J. Am. Chem. Soc.* **1999**, *121*, 5625–5632; b) D. W. Brousmiche, P. Wan, *J. Photochem. Photobiol. A* **2000**, *130*, 113–118.
- [28] a) D. P. DeCosta, N. Howell, A. L. Pincock, J. A. Pincock, S. Rifai, *J. Org. Chem.* **2000**, *65*, 4698–4795; b) J. A. Pincock, I. S. Young, *Can. J. Chem.* **2003**, *81*, 1083–1095; c) J. W. Hilborn, E. MacKnight, J. A. Pincock, P. J. Wedge, *J. Am. Chem. Soc.* **1994**, *116*, 3337–3346; d) J. A. Pincock, *Acc. Chem. Res.* **1997**, *30*, 43–49.
- [29] H. E. Zimmerman, V. R. Sandel, *J. Am. Chem. Soc.* **1963**, *85*, 915–922.
- [30] a) T. Goshima, Y. Itoh, H. Shirai, M. Kojima, *J. Photochem. Photobiol. A* **2001**, *141*, 139–145; b) T. Goshima, Y. Itoh, M. Kojima, T. Karatsu, *J. Photochem. Photobiol. A* **1999**, *127*, 75–81.
- [31] N. J. Turro, *Modern Molecular Photochemistry*, University Science Book, Sausalito, **1991**.
- [32] J. Bartl, S. Steenken, H. Mayr, R. A. McClelland, *J. Am. Chem. Soc.* **1990**, *112*, 6918–6918.
- [33] a) M. Lipson, A. A. Deniz, K. S. Peters, *J. Am. Chem. Soc.* **1996**, *118*, 2992–2997; b) M. Lipson, A. A. Deniz, K. S. Peters, *J. Phys. Chem.* **1996**, *100*, 3580–3586; c) M. Lipson, A. A. Deniz, K. S. Peters, *Chem. Phys. Lett.* **1998**, *288*, 781–784.
- [34] G. Porter, M. W. Windsor, *Nature* **1957**, *180*, 187–188.
- [35] H. C. Christensen, K. Sehested, E. J. Hart, *J. Phys. Chem.* **1973**, *77*, 983–987.
- [36] H. G. Heine, W. Hartmann, D. R. Kory, J. G. Magyar, C. E. Hoyle, J. K. McVey, F. D. Lewis, *J. Org. Chem.* **1974**, *39*, 691–698.
- [37] J. M. Masnovi, S. Sankararaman, J. K. Kochi, *J. Am. Chem. Soc.* **1989**, *111*, 2263–2276.
- [38] a) R. S. Givens, B. Matszewski, P. S. Athey, M. R. Stoner, *J. Am. Chem. Soc.* **1990**, *112*, 6016–6021; b) R. S. Givens, B. Matuszewski, *J. Am. Chem. Soc.* **1984**, *106*, 6860–6861.
- [39] C. Reichardt, *Solvent and Solvent Effect in Organic Chemistry*, VCH, Weinheim, **1988**.
- [40] a) I. E. Kochevar, P. J. Wagner, *J. Am. Chem. Soc.* **1972**, *94*, 3859–3865; b) P. J. Wagner, R. A. Leavitt, *J. Am. Chem. Soc.* **1970**, *92*, 5806–5808.
- [41] R. W. Ricci, J. M. Nesta, *J. Chem. Phys.* **1976**, *64*–65, 974–980.
- [42] a) J. C. Netto-Ferreira, W. J. Leigh, J. C. Scaiano, *J. Am. Chem. Soc.* **1985**, *107*, 2617–2622; b) J. C. Netto-Ferreira, I. G. J. Avellar, J. C. Scaiano, *J. Org. Chem.* **1990**, *55*, 89–92.
- [43] a) P. J. Wagner, M. A. Meador, B. Zhuo, B.-S. Park, *J. Am. Chem. Soc.* **1991**, *113*, 9630–9639; b) P. J. Wagner, B. Zhou, T. Hasegawa, D. L. Ward, *J. Am. Chem. Soc.* **1991**, *113*, 9640–9654; c) P. J. Wagner, B. P. Giri, J. C. Scaiano, D. L. Ward, E. Gabe, F. L. Lee, *J. Am. Chem. Soc.* **1985**, *107*, 5483–5490.
- [44] T. Wilson, A. M. Halpern, *J. Am. Chem. Soc.* **1981**, *103*, 2412–2413.
- [45] a) J. N. Moorthy, S. L. Monahan, R. B. Sunoj, J. Chandrasekhar, C. Bohne, *J. Am. Chem. Soc.* **1999**, *121*, 3093–3103; b) S. Samanta, B. K. Mishra, T. C. S. Pace, N. Sathyamurthy, C. Bohne, J. N. Moorthy, *J. Org. Chem.* **2006**, *71*, 4453–4459.
- [46] L. Giering, M. Berger, C. Steel, *J. Am. Chem. Soc.* **1974**, *96*, 953–958.
- [47] P. K. Das, K. Bobrowski, *J. Chem. Soc. Faraday Trans.* **1981**, *77*, 1009–1027.
- [48] F. D. Lewis, T. A. Hillard, *J. Am. Chem. Soc.* **1970**, *92*, 6672–6674.
- [49] R. R. Hautala, N. J. Turro, *J. Am. Chem. Soc.* **1971**, *93*, 5595–5597.
- [50] N. C. Yang, M. H. Hui, S. A. Bellard, *J. Am. Chem. Soc.* **1971**, *93*, 4056–4058.
- [51] M. Lipson, P. F. McGarry, I. V. Koptuyug, H. A. Staab, N. J. Turro, D. C. Doetschman, *J. Chem. Phys.* **1994**, *100*–101, 7504–7512.
- [52] Gaussian 98, Revision A.11.3, M. J. Frisch, G. W. Trucks, H. B. Schlegel, G. E. Scuseria, M. A. Robb, J. R. Cheeseman, V. G. Zakrzewski, J. A. Montgomery, Jr., R. E. Stratmann, J. C. Burant, S. Dapprich, J. M. Millam, A. D. Daniels, K. N. Kudin, M. C. Strain, O. Farkas, J. Tomasi, V. Barone, M. Cossi, R. Cammi, B. Mennucci, C. Pomelli, C. Adamo, S. Clifford, J. Ochterski, G. A. Petersson, P. Y. Ayala, Q. Cui, K. Morokuma, N. Rega, P. Salvador, J. J. Dannenberg, D. K. Malick, A. D. Rabuck, K. Raghavachari, J. B. Foresman, J. Cioslowski, J. V. Ortiz, A. G. Baboul, B. B. Stefanov, G. Liu, A.

Liashenko, P. Piskorz, I. Komaromi, R. Gomperts, R. L. Martin,  
D. J. Fox, T. Keith, M. A. Al-Laham, C. Y. Peng, A. Nanayakkara,  
M. Challacombe, P. M. W. Gill, B. Johnson, W. Chen, M. W. Wong,

J. L. Andres, C. Gonzalez, M. Head-Gordon, E. S. Replogle, J. A.  
Pople, Gaussian, Inc., Pittsburgh PA, **2002**.

Received: October 20, 2009  
Published online: March 26, 2010